Compressible structures in incompressible hydrodynamics and their role in turbulence onset

E.A. Kuznetsov

Lebedev Physical Institute, Moscow, Russia

Landau Institute for Theoretical Physics, Moscow, Russia

Novosibirsk State University, Novosibirsk, Russia

Nizhnii Novgorod, Nonlinear Waves - 2018, February, 27, 2018

Joined with:

D.S. Agafontsev (Shirshov Institute & NSU),

A.A. Mailybaev (IMPA, Brazil),

E.V. Sereshchenko (NSU & Khristianovich ITAM, Novosibirsk)

OUTLINE

- Motivation: Collapse and the Kolmogorov-Obukhov theory
- Vortex line representation (VLR)
- Compressibility of VLR and folding of vortex lines
- Numerical experiment
- Tendency to breaking in 2D turbulence
- Numerical experiments for 2D decay turbulence
- 2D turbulence with pumping and viscous-type damping

Motivation: Collapse and the Kolmogorov-Obukhov theory

- According to the Kolmogorov-Obukhov theory (1941) velocity fluctuations at spatial scales l from the inertial range obey the power-law $\langle|\delta v|\rangle \propto \varepsilon^{1/3} l^{1/3}$, where ε is the mean energy flux from large to small scales. This formula is easily obtained from the dimensional analysis.
- Similarly, fluctuations for the vorticity field $\omega = \nabla \times \mathbf{v}$ diverge at small scales as $\langle|\delta\omega|\rangle \propto \varepsilon^{1/3} l^{-2/3}$, while the time of energy transfer from the energy-contained scale l_E to the viscous ones is finite and estimated as $T \sim l_E^{2/3} \varepsilon^{-1/3}$.
- These two relations allow to link the Kolmogorov spectrum formation with the blowup in the vorticity field (collapse).

Motivation: Collapse and the Kolmogorov-Obukhov theory

- Kolmogorov's arguments assume locality of interaction and isotropy of the turbulence in the inertial interval. This implies that the dynamics at these scales can be described by the Euler equations and the emergence of the Kolmogorov energy spectrum can be expected before the viscous scales are excited, i.e., in a fully inviscid flow.
- This conjecture was verified numerically in our previous papers (2015, 2016, 2017), where we showed that the Kolmogorov spectrum is developed through the formation of pancake-like structures of enhanced vorticity. Such pancakes can be treated as coherent structures.
- At the stage of turbulence onset turbulence is far from isotropic, its spectrum contains a few number of jets. Each jet corresponds to its own pancake.

Motivation: Collapse and the Kolmogorov-Obukhov theory

- We also established numerically the asymptotic Kolmogorov-type scaling,

$$\omega_{\max}(t) \propto \ell(t)^{-2/3},$$

  between the vorticity maximum on the pancake and the pancake thickness.

- No tendency to finite-time blowup was observed for generic initial conditions, with nearly exponential growth of vorticity in time.

- In the present paper we develop a new concept of folding for continuously distributed vortex lines.

Motivation: Collapse and the Kolmogorov-Obukhov theory

- The underlying idea that enables the folding phenomenon is that the “flow” of continuously distributed vortex lines is compressible, despite the incompressibility of the fluid: the vortex lines representation (VLR), E.K.& V. Ruban, 1998. Our new theory based on the VLR explains the $2/3$-law as a result of the classical fold catastrophe.
- The discussed approach is applicable for a larger class of “frozen-in-fluid” fields advected by incompressible fluid, for instance, the magnetic field in MHD or the di-vorticity field for 2D Euler.
- By means of a new adaptive numerical scheme based on the VLR we observed numerically the compressible character of continuously distributed vortex lines and verified the details of the folding phenomenon.

Vortex line representation (VLR)

Consider a frozen-in-fluid divergence-free field $\mathbf{B}$, defined from the following equation:

$$\frac{\partial \mathbf{B}}{\partial t} = \mathrm{rot}(\mathbf{v} \times \mathbf{B}), \;\; \mathrm{div}\, \mathbf{v} = 0.$$

Examples of such fields are the vorticity $\omega = \nabla \times \mathbf{v}$ for the 3D Euler equations, the magnetic field in (ideal) MHD and the divorticity field $\mathbf{B} = \nabla \times \omega$ for 2D Euler hydrodynamics. Such a $\mathbf{B}$-field line can only be changed by the velocity component $\mathbf{v}_n$ perpendicular to $\mathbf{B}$. Now we introduce a new type of trajectories given by the normal velocity component as

$$\frac{d\mathbf{x}}{dt} = \mathbf{v}_n(\mathbf{x}, t), \;\; \mathbf{x}|_{t=0} = \mathbf{a}.$$

Vortex line representation (VLR)

Because of frozenness of the field $\mathbf{B}$ a solution $\mathbf{x} = \mathbf{x}(\mathbf{a}, t)$ describes the motion of field lines. In terms of this mapping, Eq. for $\mathbf{B}$ admits explicit integration

$$\mathbf{B}(\mathbf{x}, t) = \frac{\widehat{J}\,\mathbf{B}_0(\mathbf{a})}{J}, \quad \widehat{J}(\mathbf{a}, t) = \left[\frac{\partial x_i}{\partial a_j}\right], \quad J = \det \widehat{J},$$

where $\mathbf{B}_0(\mathbf{a})$ is the initial field at $t = 0$ (analogous to the Cauchy invariant) and $\widehat{J}$ is the Jacobi matrix of the mapping. From the equations of motion for the vortex lines follows the following equation for the Jacobian (the Liouville formula):

$$\frac{dJ}{dt} = \text{div}\, \mathbf{v_n} \cdot J.$$

Vortex line representation (VLR)

In the general situation, div $\mathbf{v_n} \neq 0$. By this reason, the Jacobian as a measure of the volume changing can take arbitrary values, in particular, can vanish.

The inverse Jacobian, $n = 1/J$, has the meaning of density of B-lines and satisfies the continuity equation

$$\frac{\partial n}{\partial t} + \mathrm{div}(n\mathbf{v}_n) = 0.$$

One more useful relation. Consider the maximal value of B_{max}. Then one can easily get

$$\frac{dB_{max}}{dt} = B_{max}(\tau(\nabla\tau)\mathbf{v})$$

where $\tau = \mathbf{B}/|B|$. From another side div $\mathbf{v_n} = -$div $\mathbf{v}_\tau$ that approximately gives at the maximal point $B_{max}J \approx$ const.

Vortex line representation (VLR)

In the case of the 3D hydrodynamics, Eqs. written for the vorticity $\mathbf{B} = \omega$ together with the relation $\omega = \nabla \times \mathbf{v}$ are called the vortex line representation (VLR), and form a complete set of equations equivalent to the Euler equations. However, these equations are written in mixed Eulerian ($\mathbf{x}$-space) and Lagrangian ($\mathbf{a}$-space) variables. For numerical study, we now rewrite all the equations using the Eulerian variables.

Let $\mathbf{a} = \mathbf{a}(\mathbf{x}, t)$ be the inverse mapping. This mapping obeys the equation

$$\frac{\partial \mathbf{a}}{\partial t} + (\mathbf{v}_n \cdot \nabla)\mathbf{a} = 0.$$

Vortex line representation (VLR)

Eq. for the vorticity $\mathbf{B} = \omega$ can be rewritten in the form

$$\omega_i(\mathbf{x}, t) = \frac{1}{2}\varepsilon_{ijk}\,\varepsilon_{\alpha\beta\gamma}\,\omega_{0\alpha}(\mathbf{a})\,\frac{\partial a_\beta}{\partial x_j}\,\frac{\partial a_\gamma}{\partial x_k}.$$

Here $\omega_0(\mathbf{a})$ is the initial vorticity at $t = 0$. The two equations together with the relations

$$\mathbf{v} = \mathrm{rot}^{-1}\omega = -\Delta^{-1}\left(\nabla \times \omega\right), \quad \mathbf{v}_n = \mathbf{v} - \frac{(\mathbf{v} \cdot \omega)}{\omega^2}\omega$$

for the velocity and the normal velocity represent complete VLR system of equations written in the Eulerian coordinates $(\mathbf{x}, t)$.

Folding of vortex lines

REMARK 1: Wave breaking, as blowup, is well known for compressible flows resulting in appearance of shocks, which can be considered as the formation of folds. Breaking in gasdynamics is possible due to compressible character of the mapping.

REMARK 2: Breaking/folding of vortex lines is impossible in 2D and for cylindrically symmetric flows without swirl (Majda, 1990) because $\omega \perp \mathbf{v}$ and div $\mathbf{v}_n = 0$, and consequently $J = 1$.

Thus, breaking/folding of vortex lines is 3D phenomenon.

Up to now it has not been known whether this process happens in a finite or infinite time.

Folding of vortex lines

In our numerics exponential increasing of the vorticity maximum and formation around this maximum a structure of the pancake type with exponential decreasing of its width were observed, instead of blow-up. Such structures appear around each vorticity maximum and are shown to have self-similar behavior. (First numerics by M. Brachet, et. el. (1992).)

Geometrically breaking results in touching of vortex lines (in a finite or infinite time).

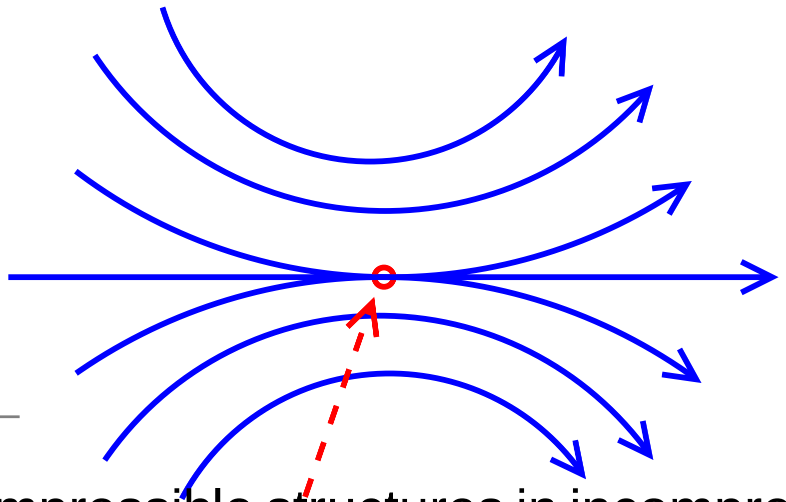

Folding of vortex lines

Let us assume that breaking/folding takes place. Consider the equation $J(\mathbf{a},t)=0$ and find its positive roots $t=\tilde{t}(\mathbf{a})>0$. Then the collapse (or touching) time will be

$$t_0=\min_a \tilde{t}(\mathbf{a}).$$

Near the minimal point $\mathbf{a}=\mathbf{a}_0$ as the expansion of J takes the form:

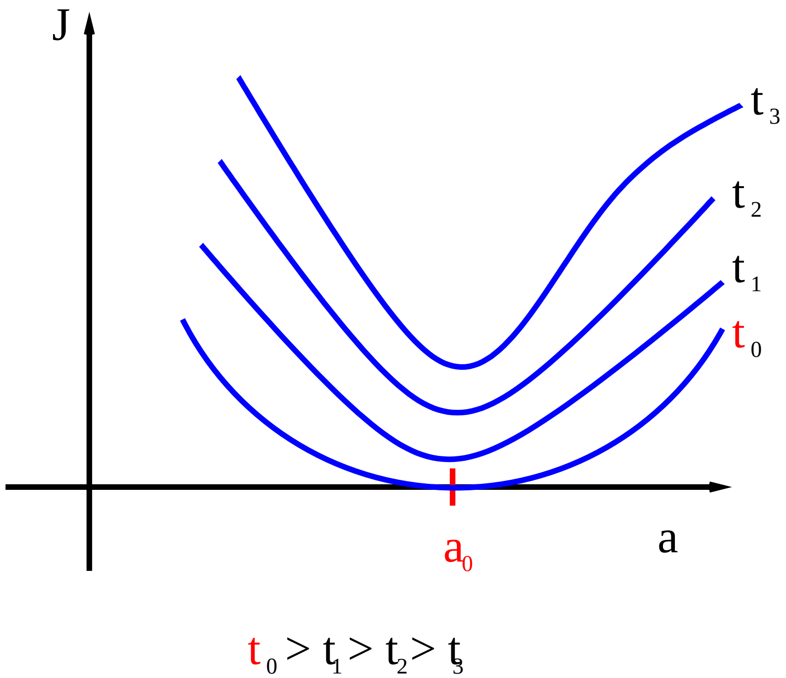

$J(a,t)=\alpha\tau(t)+\gamma_{ij}\Delta a_i\Delta a_j$

- concavity condition

$\alpha>0$, $\tau(t)\to 0$ as $t\to t_0$,

γ_{ij} is positive definite (non-degenerate) time independent matrix,

$\Delta\mathbf{a}=\mathbf{a}-\mathbf{a}_0$.

Self-similar asymptotics

REMARK: The assumption about linear dependence of J_{min} on $\tau(t)$ is familiar to the Landau assumption in his theory of the second-order phase transitions.

This expansion results in the self-similar asymptotics for vorticity:

$$\omega(\mathbf{r},t) = \frac{(\omega_{\mathbf{0}}(\mathbf{a})\cdot\nabla_a)\mathbf{r}|_{a_0}}{\tau(\alpha+\gamma_{ij}\eta_i\eta_j)}, \quad \eta = \frac{\Delta a}{\tau^{1/2}}.$$

Now the main problem is

to transform from the auxiliary a-space to the physical $\mathbf{r}$-space.

Self-similar asymptotics

Consider first the 1D case when

$$J = \frac{\partial x}{\partial a} = \alpha\tau + \gamma a^2 \quad \to x = \alpha\tau a + \frac{1}{3}\gamma a^3.$$

Thus, $a \sim \tau^{1/2}, \ x \sim \tau^{3/2}$, i.e. in the physical space compression happens more rapidly than in the space of Lagrangian markers !! At distances $\gamma a^2 \gg \alpha\tau$ we have the time-independent asymptotics,

$$J \sim x^{2/3}.$$

Thus, any changes happen at the region $\gamma a^2 \leq \alpha\tau$.

Self-similar asymptotics

3D case

The Jacobian $J = \lambda_1\lambda_2\lambda_3 \to 0$ means that one eigenvalue, say, $\lambda_1 \to 0$ and $\lambda_2, \lambda_3 \to$ const as $t \to t_0$ and $a \to a_0$. Hence it follows that near singular point there are two different self similarities:

along "soft" (λ_1) direction $x_1 \sim \tau^{3/2}$ (like in 1D);

along "hard" (λ_2, λ_3) directions $x_{2,3} \sim \tau^{1/2}$,

so that

$$\omega = \frac{1}{\tau}\mathbf{g}\left(\frac{x_1}{\tau^{3/2}}, \frac{x_\perp}{\tau^{1/2}}\right).$$

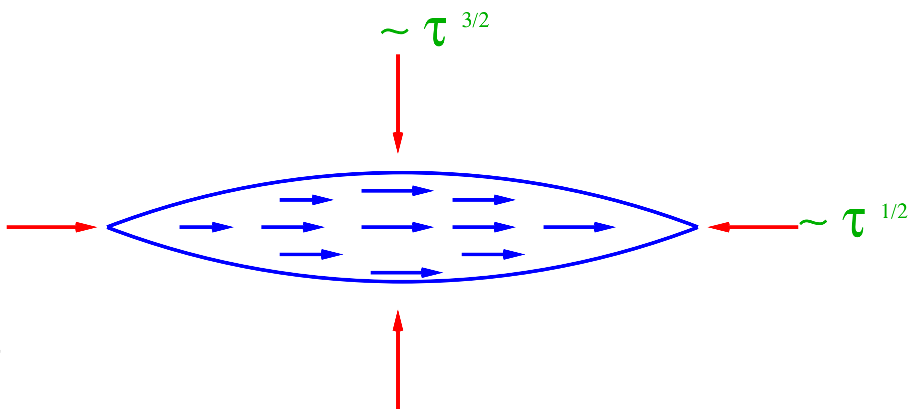

This results in formation

of pancake structure

(compare with Zeldovich)

Self-similar asymptotics

As $\tau \to 0$ when $\gamma_{ij}\Delta a_i \Delta a_j \gg \alpha\tau$ the vorticity has a time-independent, very anisotropic distribution. The main dependence of ω is connected with x_1-direction:

$$\omega \approx \frac{\mathbf{b}}{x_1^{2/3}}$$

with $\mathbf{b} =$ const and KOLMOGOROV index $2/3$!.
This dependence is realized everywhere except regions between two cubic paraboloids $-cx_\perp^3 < x_1 < cx_\perp^3$ In this narrow region vorticity at $\tau = 0$ behaves like

$$\omega \approx \frac{\mathbf{b_1}}{x_\perp^2}.$$

Self-similar asymptotics

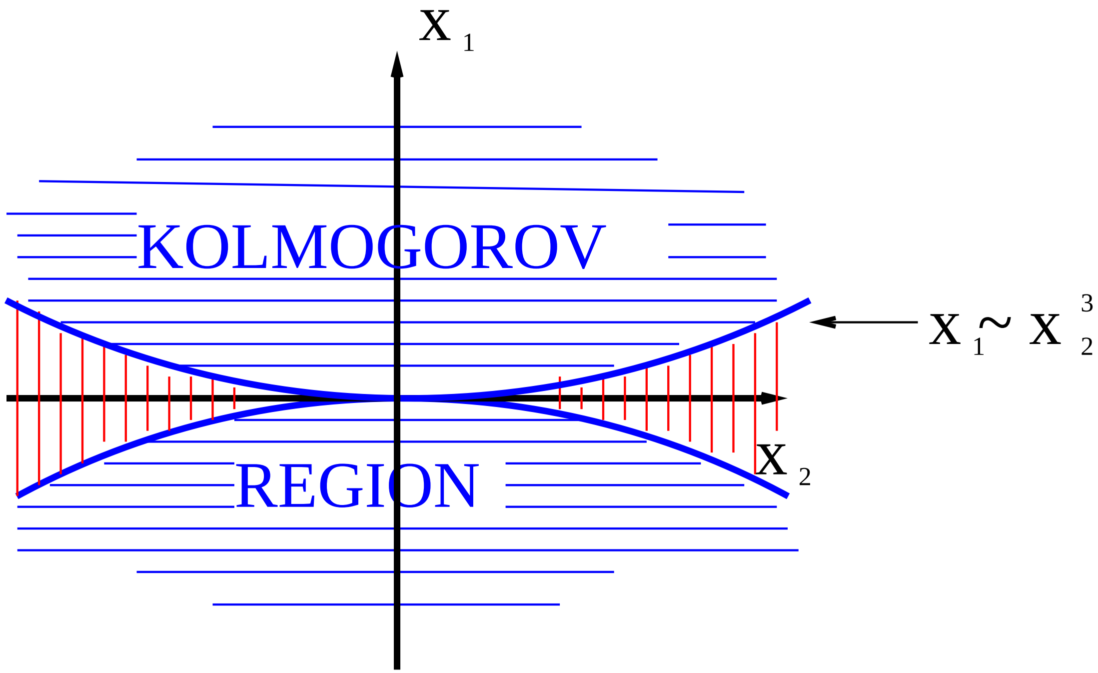

In Kolmogorov region the vorticity can be estimated as

$$\omega \sim \frac{\epsilon^{1/3}}{x_1^{2/3}}$$

where $\epsilon \sim \omega_0^3 L^2,\ L \sim \gamma^{-1/2}$.

VLR for exact solution

As it was shown by us (JFM, **813**, R1 (1-10) (2017)) 3D Euler has exact solution which in Cartesian coordinates has the form

$$\mathbf{v}(\mathbf{x},t) = -\omega_{\max}(t)\,\ell_1(t)\,f\left(\frac{x_1}{\ell_1(t)}\right)\mathbf{n}_3 + \begin{pmatrix} -\beta_1(t)\,x_1 \\ \beta_2(t)\,x_2 \\ \beta_3(t)\,x_3 \end{pmatrix},$$

$$\omega(\mathbf{x},t) = \omega_{\max}(t) f'\left(\frac{x_1}{\ell_1(t)}\right)\mathbf{n}_2.$$

Here $\omega_{\max}(t)$ and $\ell_1(t)$ are the vorticity maximum and the pancake thickness, $f(x_1)$ is arbitrary smooth function.

VLR for exact solution

- $\beta_1(t)$, $\beta_2(t)$ and $\beta_3(t)$ are given by

$$\beta_1 = -\dot{\ell}_1/\ell_1, \quad \beta_2 = \dot{\omega}_{\max}/\omega_{\max}, \quad -\beta_1 + \beta_2 + \beta_3 = 0.$$

- There exists the analog of this solution by Lundgren (1982) which describes axi-symmetric flow. But nobody before us has found the 1D (pancake) solution.
- This solution has infinite energy in $\mathbb{R}^3$ and allows for an arbitrary time-dependency of $\omega(t)$ and $\ell_1(t)$, in particular, the one leading to a finite-time blowup.

VLR for exact solution

- It can be extended for the Navier–Stokes equations with kinematic viscosity ν, if the function $f(\xi, t)$ changes with time as $f_t - \frac{\nu}{\ell_1^2} f_{\xi\xi} = 0$.
- Comparison of this solution for 3D Euler with the simulations gives a good agreement at the pancake region for $\omega_{\max}(t) \propto e^{t/T_\omega}$ and $\ell_1(t) \propto e^{-t/T_\ell}$.
- The velocity component normal to vorticity:

$$\mathbf{v}_n(\mathbf{x}, t) = -\omega_{\max}(t)\,\ell_1(t)\,f\left(\frac{x_1}{\ell_1(t)}\right)\mathbf{n}_3 + \begin{pmatrix} -\beta_1 x_1 \\ 0 \\ \beta_3 x_3 \end{pmatrix}.$$

VLR for exact solution

- For exponential pancake development the VLR mapping is written as

$$x_1 = a_1\, e^{-\beta_1 t}, \quad x_2 = a_2, \quad x_3 = a_3\, e^{\beta_3 t} - f(a_1)\,\frac{\sinh(\beta_3 t)}{\beta_3},$$

with the corresponding Jacobi matrix,

$$\hat{J}(\mathbf{a},t) = \left[\frac{\partial x_i}{\partial a_j}\right] = \begin{pmatrix} e^{-\beta_1 t} & 0 & 0 \\ 0 & 1 & 0 \\ -f'(a_1)\,\frac{\sinh(\beta_3 t)}{\beta_3} & 0 & e^{\beta_3 t} \end{pmatrix}, \quad J(\mathbf{a},t) = \det \hat{J} = e^{-\beta_2 t}$$

VLR for exact solution

- Respectively, for vorticity we have

$$\omega(\mathbf{x},t) = \frac{\widehat{J}\,\omega_0(\mathbf{a})}{J},$$

that coincides with our solution.
Hence the Jacobian is inverse-proportional to the vorticity $J(t) \propto 1/\omega_{\max}(t)$, and does not depend on spatial coordinates.

Numerical experiment

We use two numerical schemes based on direct integration of the Euler equations for ω and the VLR formulation in the periodic box $\mathbf{r} = (x, y, z) \in [-\pi, \pi]^3$ using the pseudo-spectral method with high-order Fourier filtering. During simulations, the number of nodes is adapted independently along each coordinate providing an optimal anisotropic rectangular grid. We tested several large-scale initial conditions in the form of random truncated (up to second harmonics) Fourier series considered as a perturbation of the shear flow $\omega_x = \sin z,\ \omega_y = \cos z,\ \omega_z = 0$. This paper is based on one selected simulation with the final grid $486 \times 1024 \times 2048$.

Numerical experiment: direct integration

Evolution of local vorticity maximums (logarithmic vertical scale). Green line shows the global maximum, dashed red line indicates the slope $\propto e^{t/T_\omega}$ with $T_\omega = 2$.

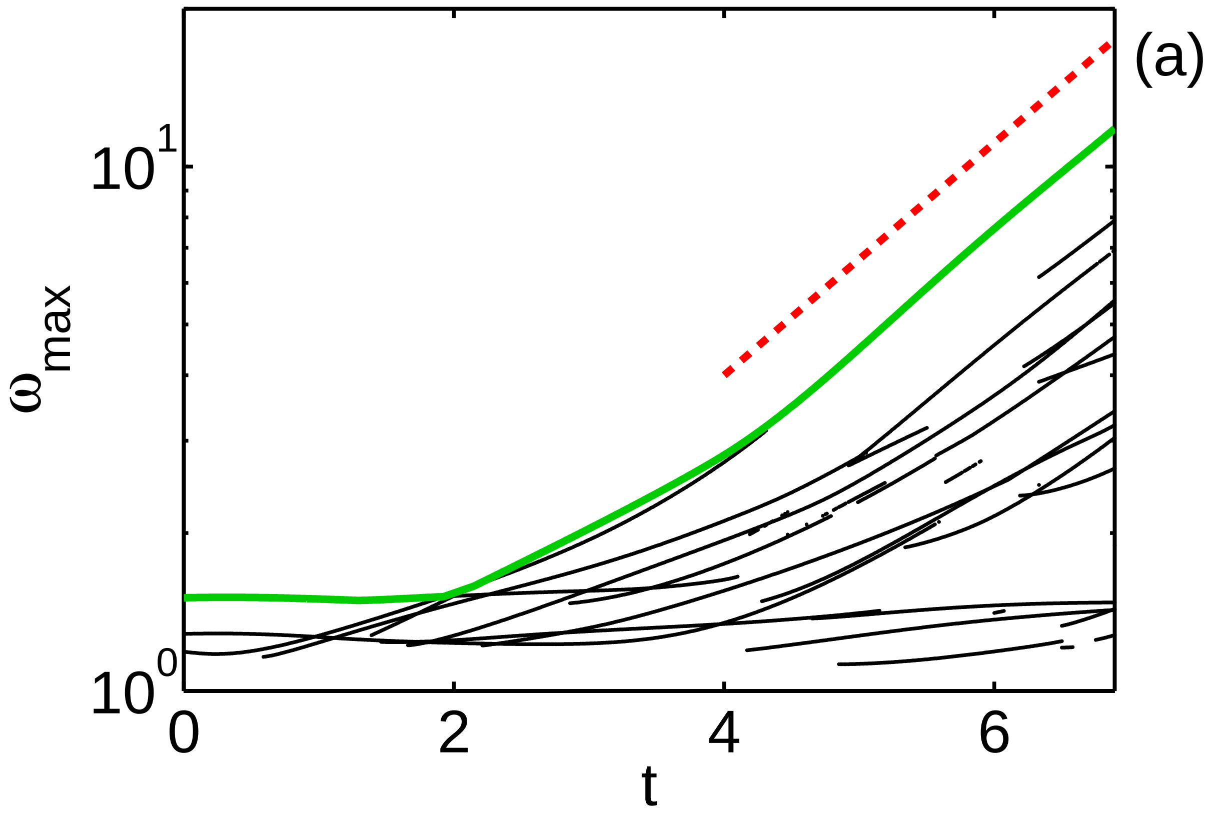

Numerical experiment: direct integration

Evolution of characteristic spatial scales ℓ_1 (black), ℓ_2 (blue) and ℓ_3 (red) for the global vorticity maximum. Dashed red line indicates the slope $\propto e^{-t/T_\ell}$ with $T_\ell = 1.4$.

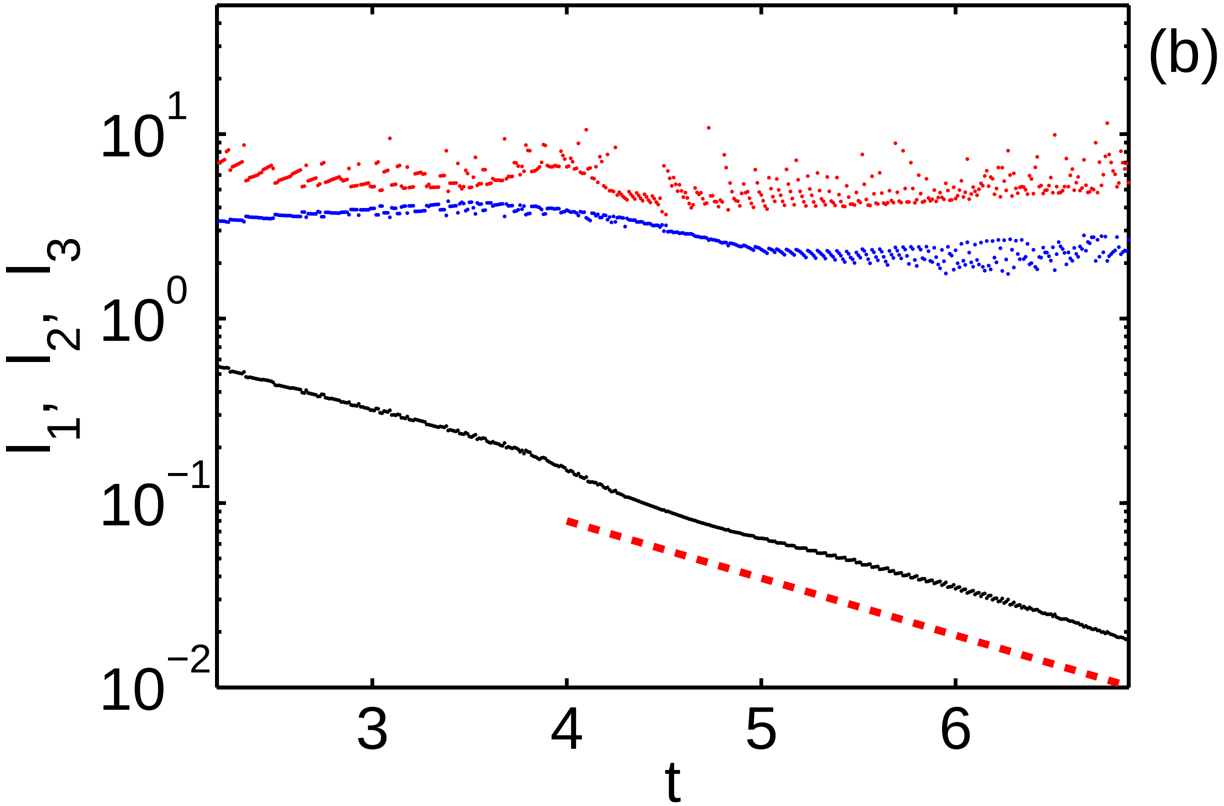

Numerical experiments: direct integration

Vorticity local maximums $\omega_{\max}(t)$ vs. lengths $\ell_1(t)$ during the evolution of the pancake structures. Green line shows the global maximum, red circles mark local maximums at the final time. Dashed red line indicates the power-law $\omega_{\max} \propto \ell_1^{-2/3}$.

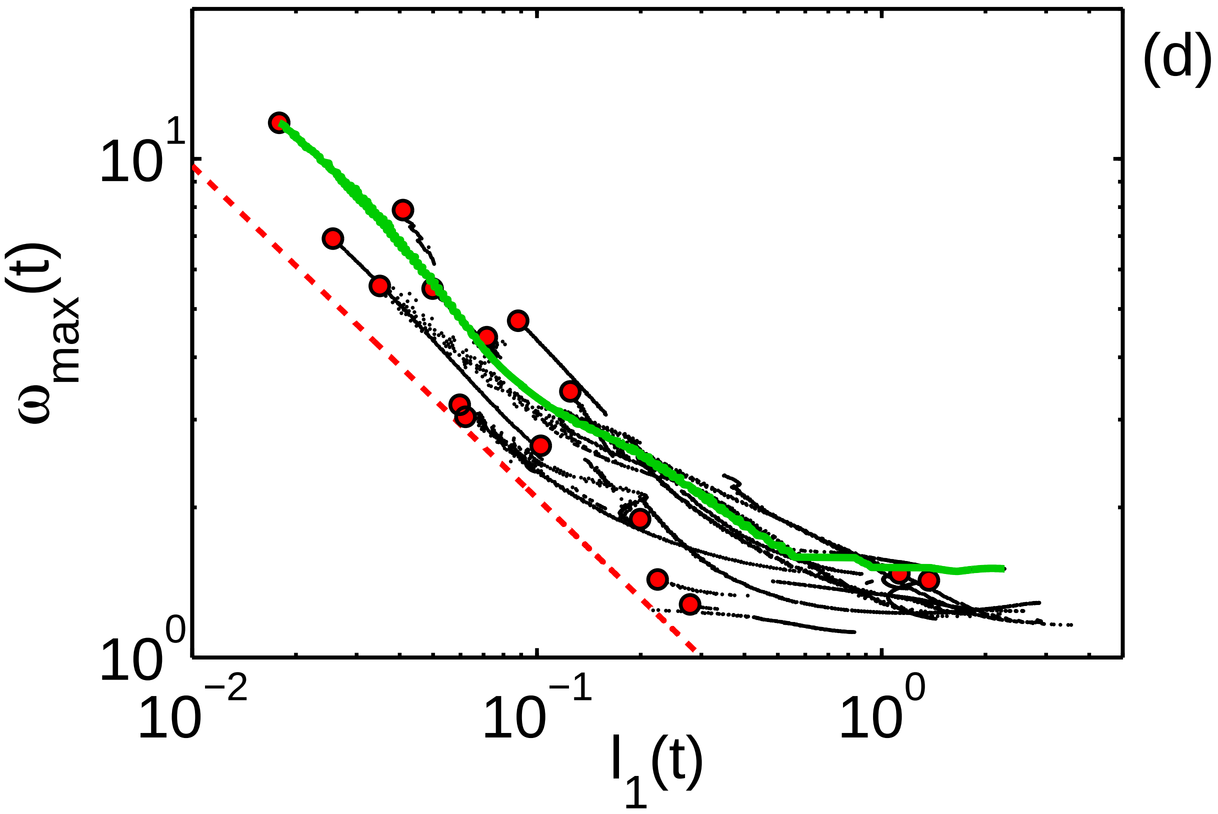

Numerical experiments: direct integration

Components of the vorticity vector $\omega = (\omega_1, \omega_2, \omega_3)$ as functions of a_1 perpendicular to the pancake, at the final time.

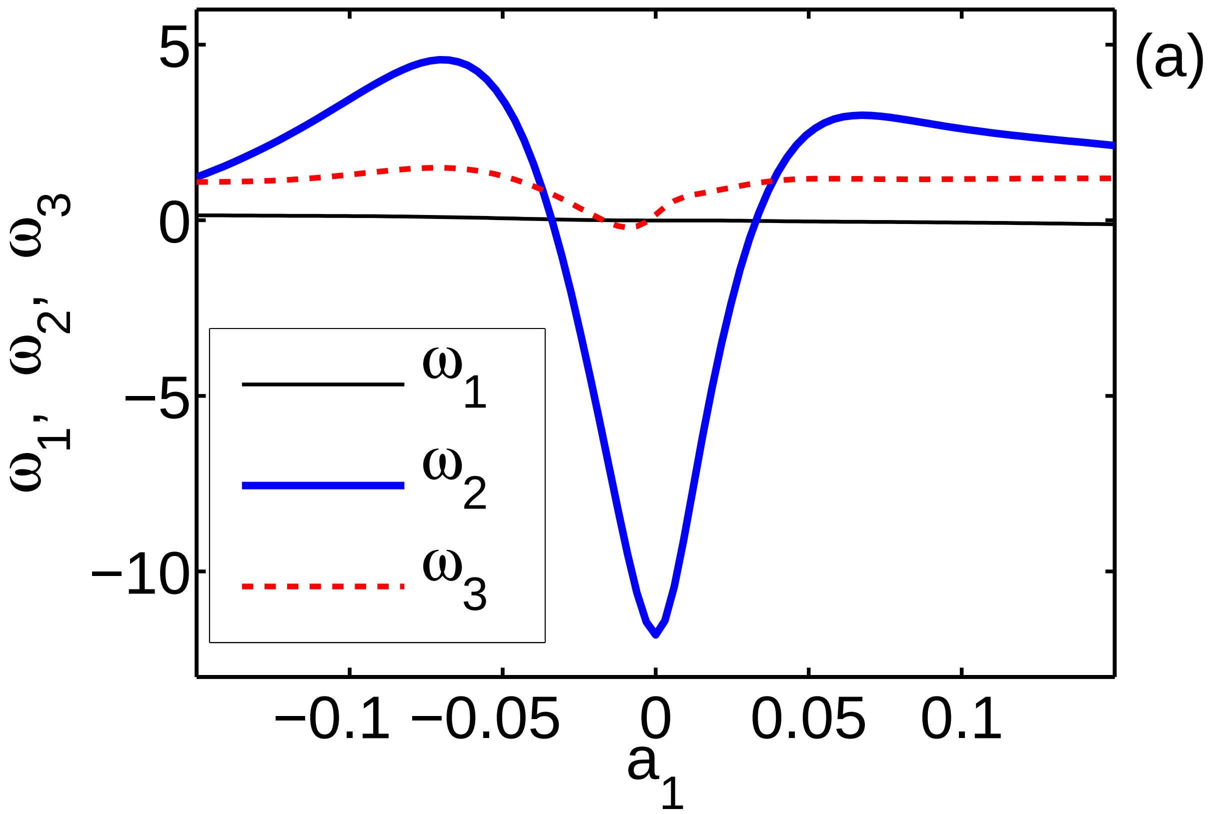

Numerical experiment: direct integration

Vorticity component $\omega_2/\omega_{\max}$ vs. coordinate a_1/ℓ_1 at different times, demonstrating the self-similarity from $\ell_1(5) = 0.064$ to $\ell_1(6.89) = 0.018$.

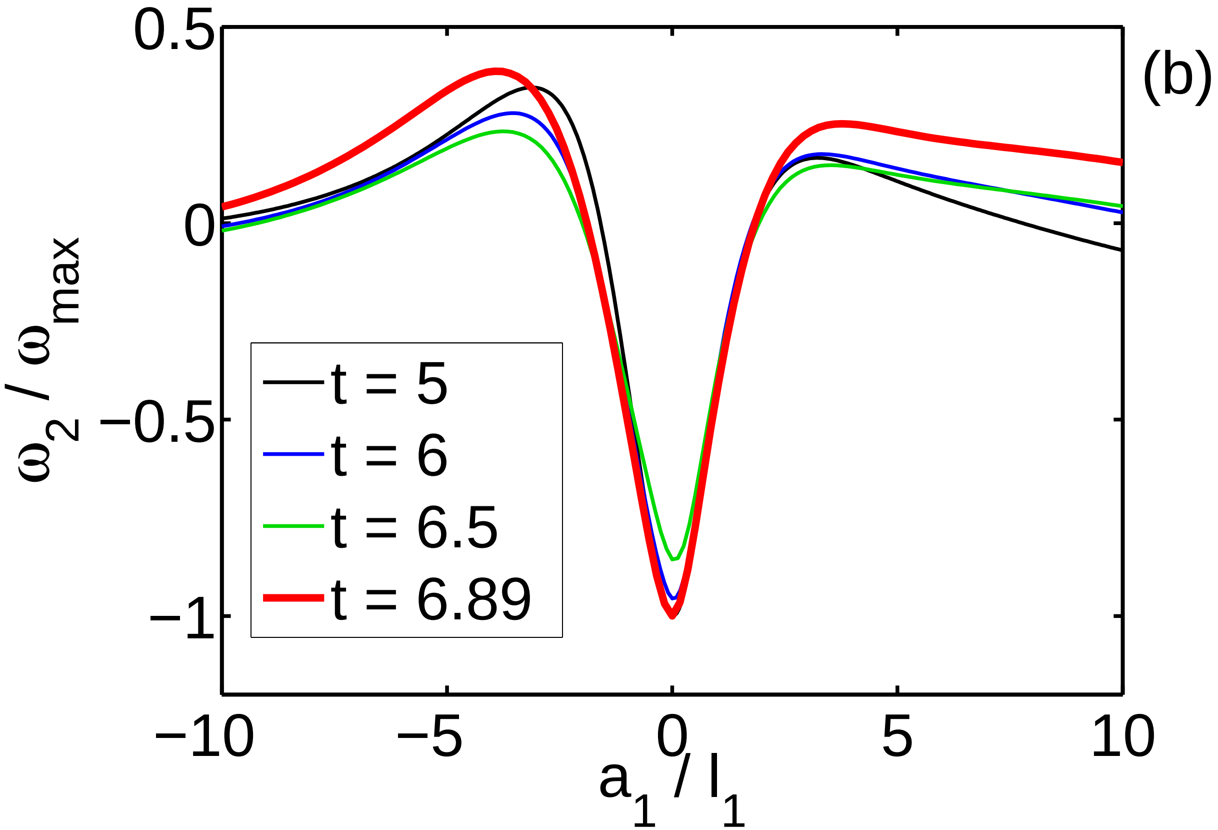

Numerical experiment: direct integration

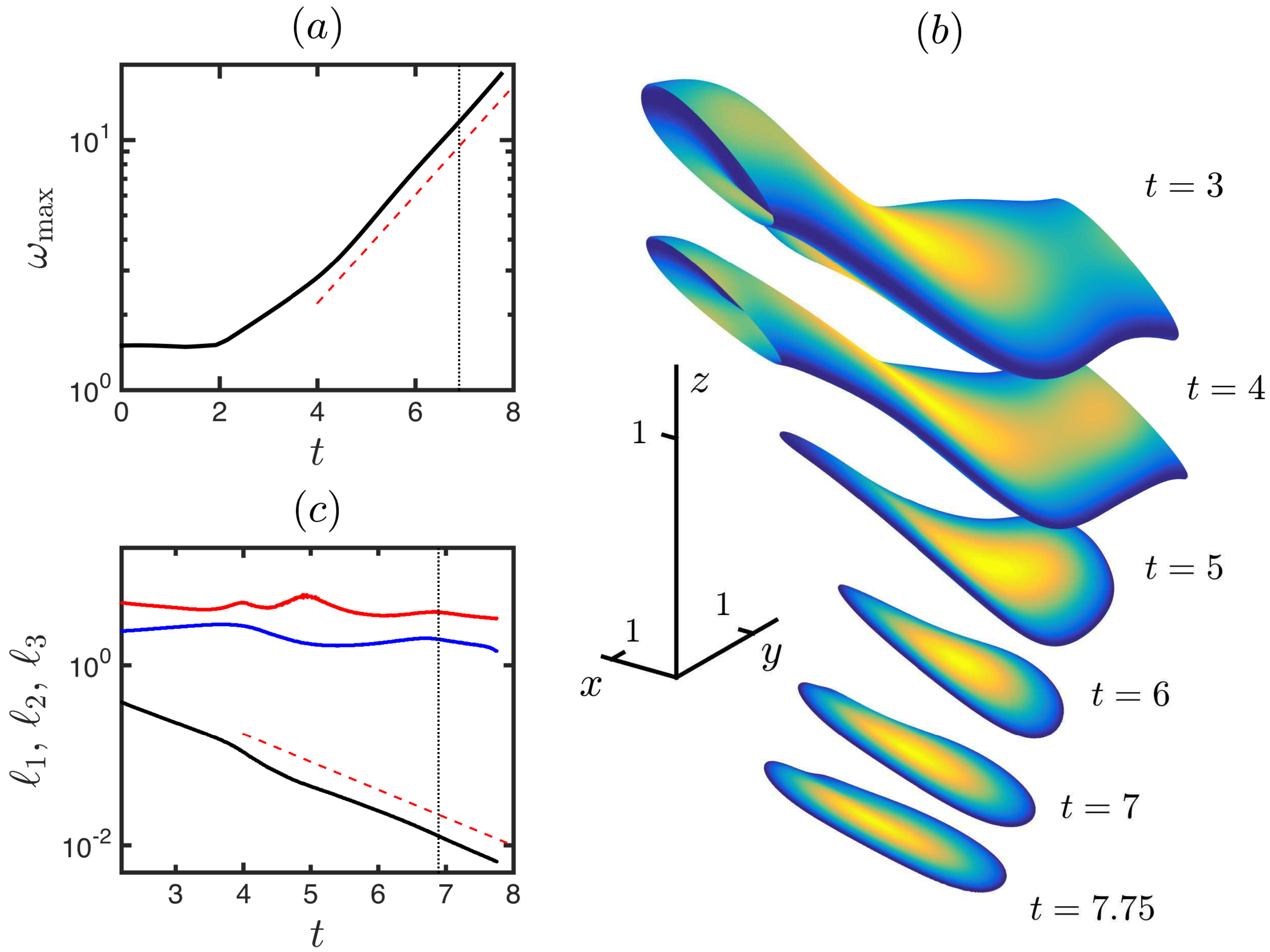

Evolution of pancake (right), dependences of ω_{max} and $\ell_{1,2,3}$ (left).

Numerical experiment

- By use of the direct integration we found that at the maximal vorticity point

$$\frac{1}{\omega_{max}}\frac{d\omega_{max}}{dt} \approx -\mathrm{div}\,\mathbf{v_n}.$$

This means that the main contribution into the vorticity maximum comes from the denominator,

$$\omega(\mathbf{r},t) = \frac{(\omega_0(\mathbf{a})\cdot\nabla_a)\mathbf{r}(\mathbf{a},t)}{J(\mathbf{a},t)}.$$

- By means of the VLR scheme it was demonstrated decreasing of the Jacobian. This means that formation of the pancake structures can be considered as folding breaking of the vorticity lines.

Direct integration: compressibility

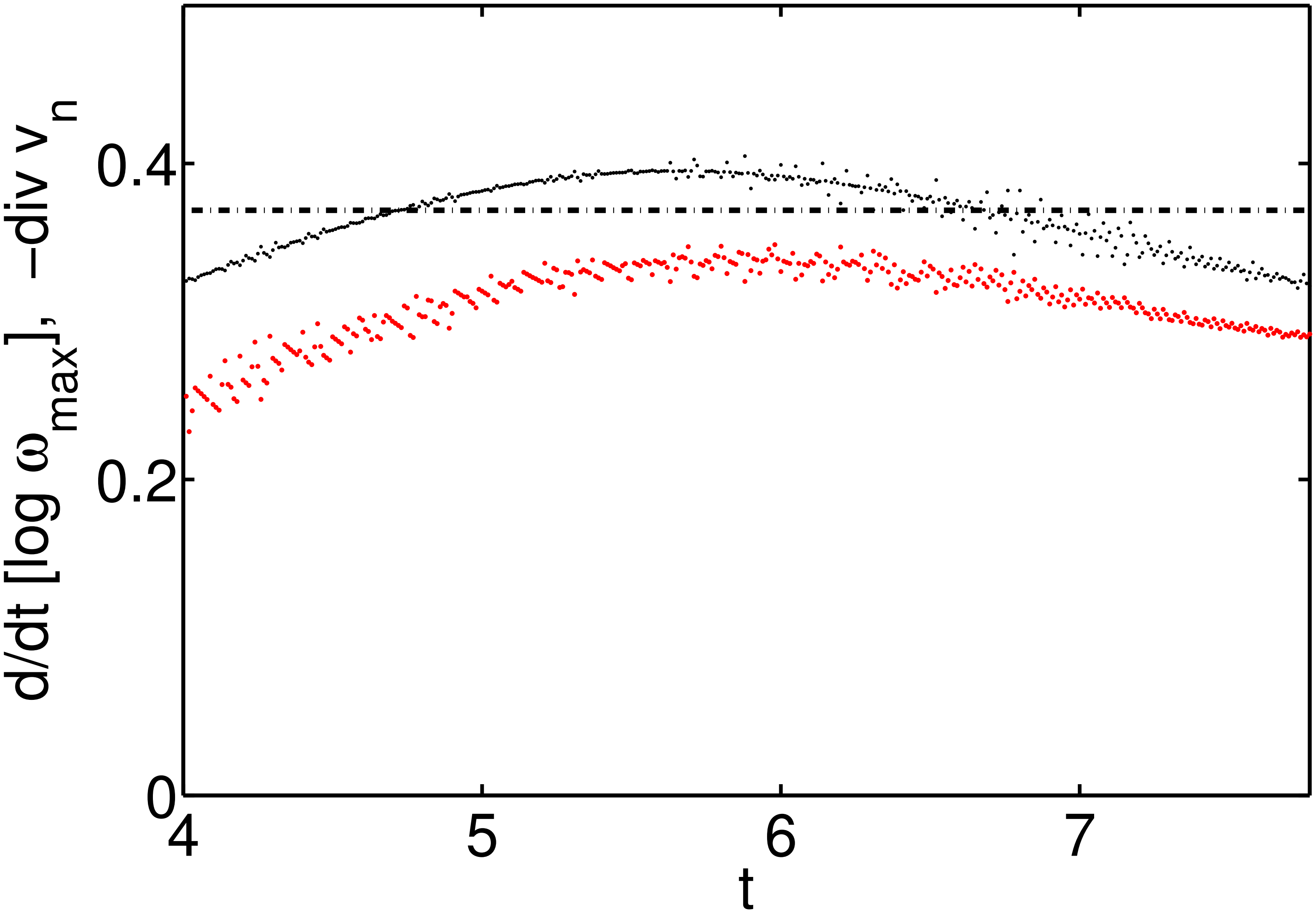

Comparison of $d \log \omega_{max}/dt$ and $-\mathrm{div}\, \mathbf{v_n}$.

Numerical experiment: compressibility

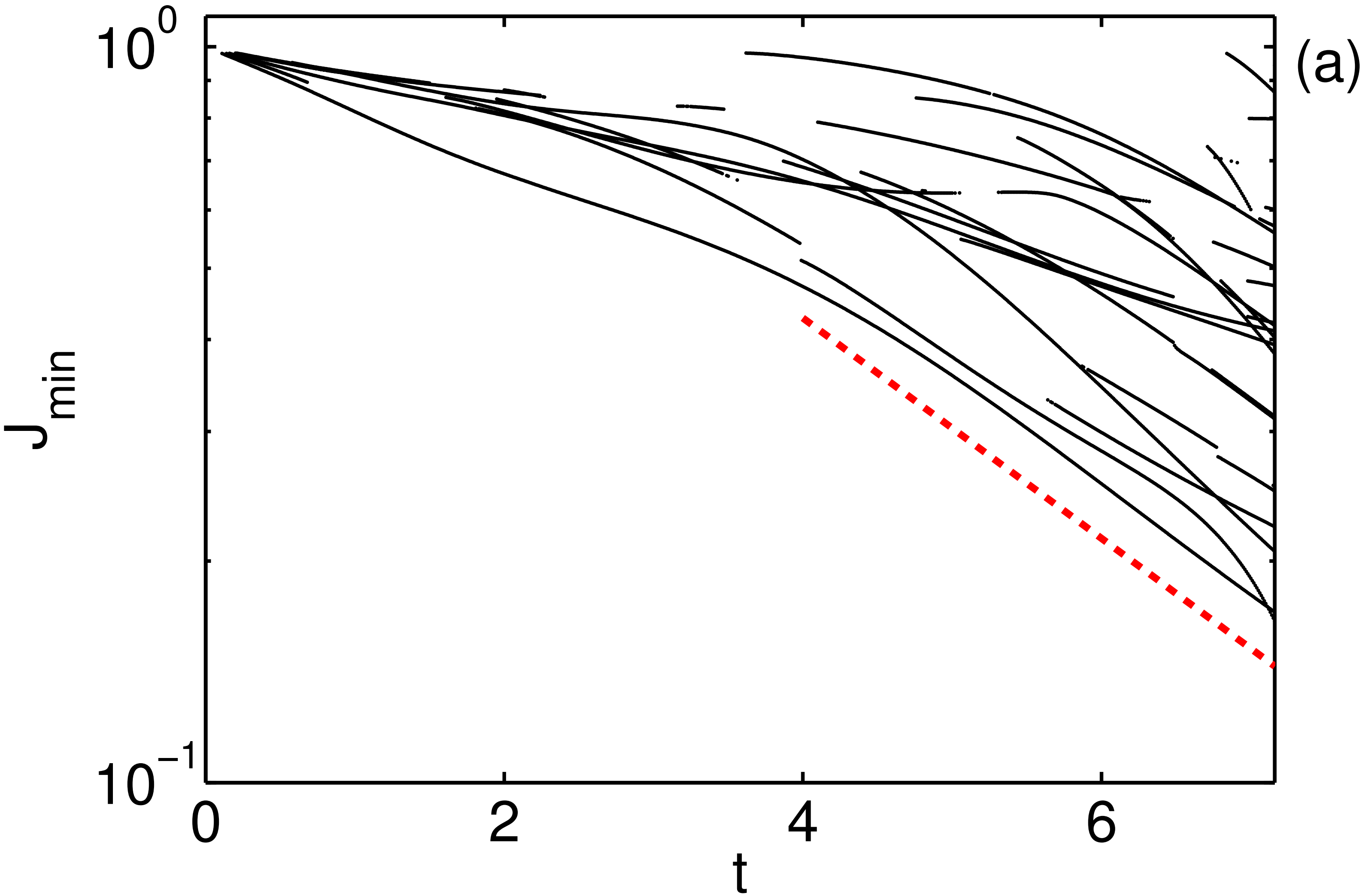

Decreasing of the Jacobian (VLR scheme)

Numerical experiment: compressibility

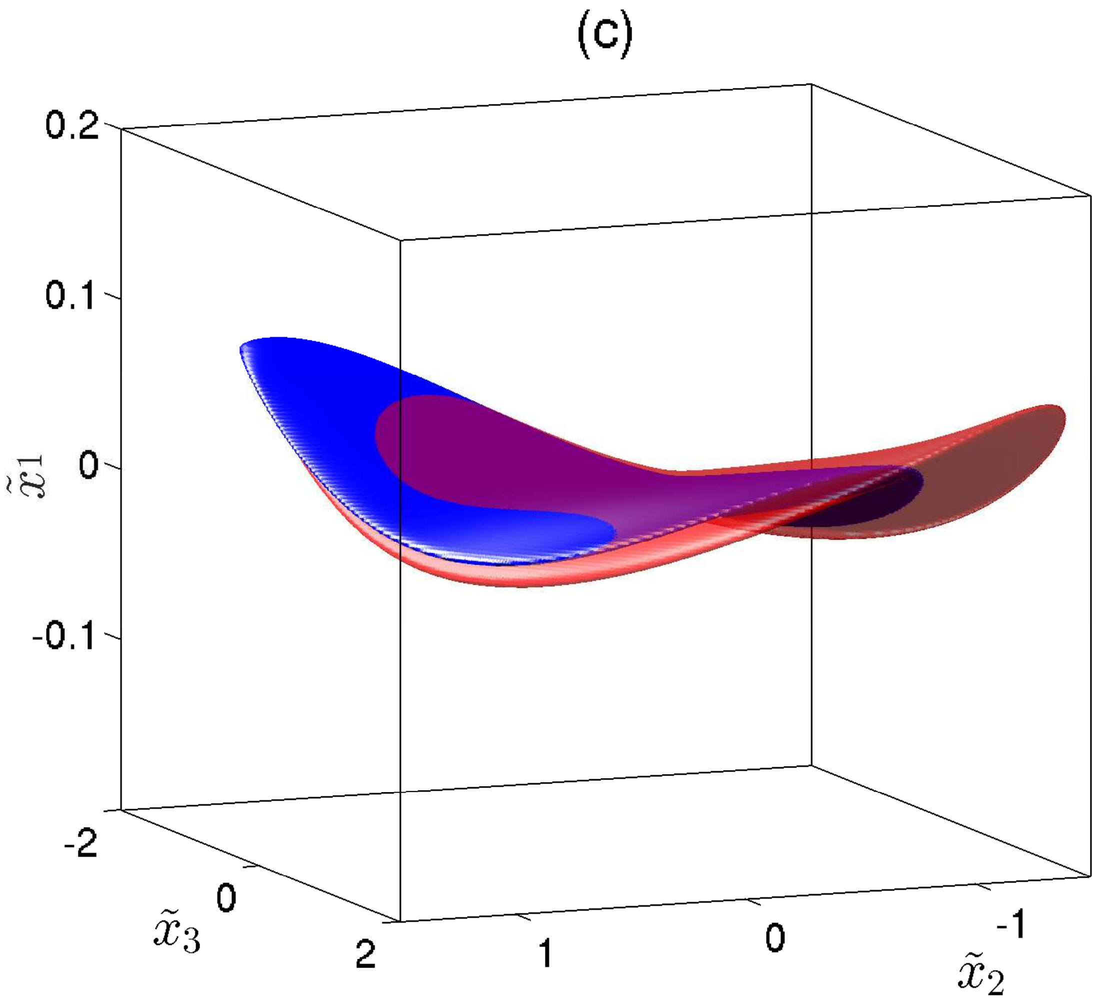

Isosurfaces $|\boldsymbol{\omega}| = 0.8\,\omega_{\max}$ (red) and $J = 1.25\,J_{\min}$ (blue) at $t = 7.5$ (VLR simulation)

Numerical experiment: compressibility

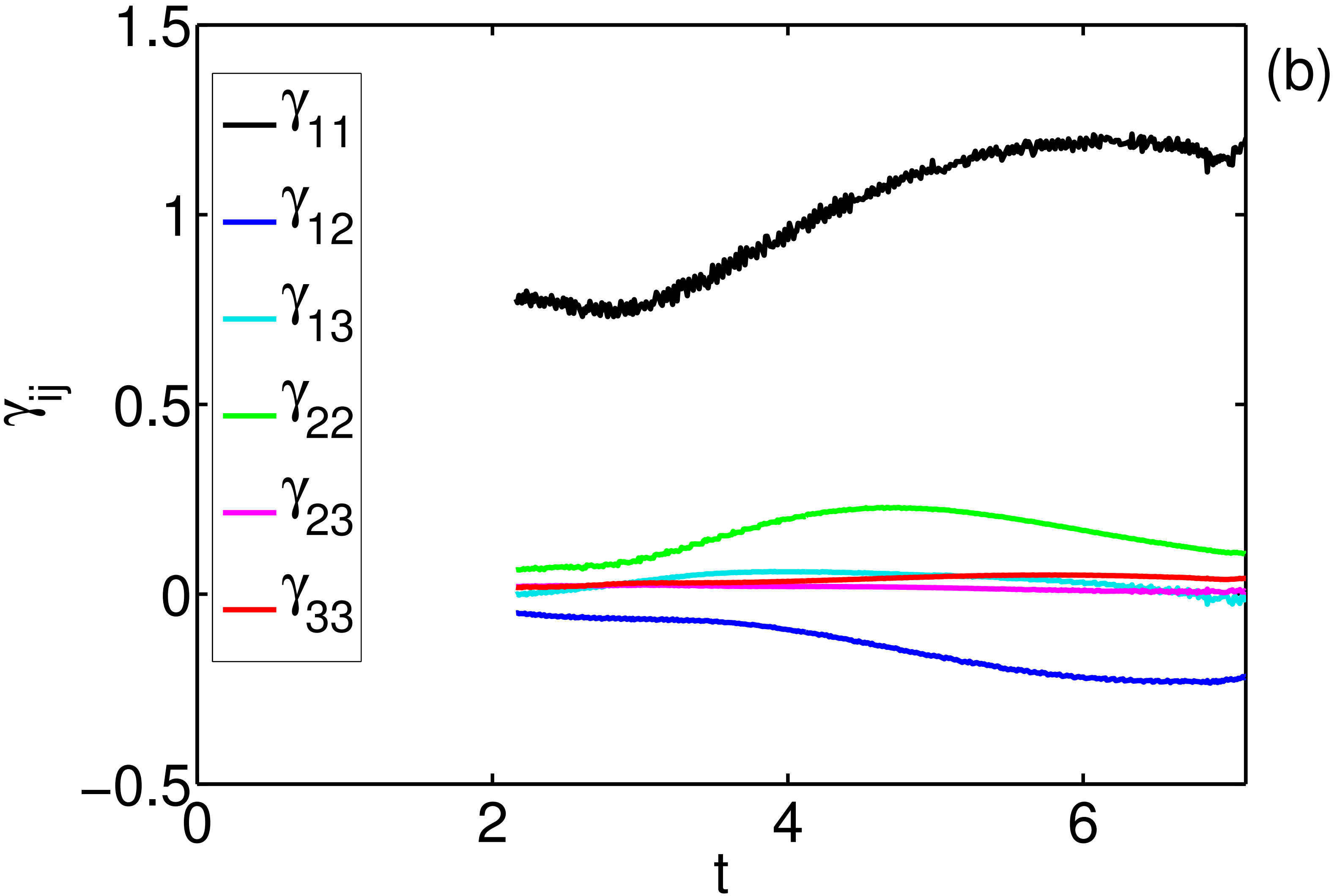

Behavior of γ_{ij} with time.

Numerical experiment

Energy spectrum at different times demonstrating the Kolmogorov power-law.

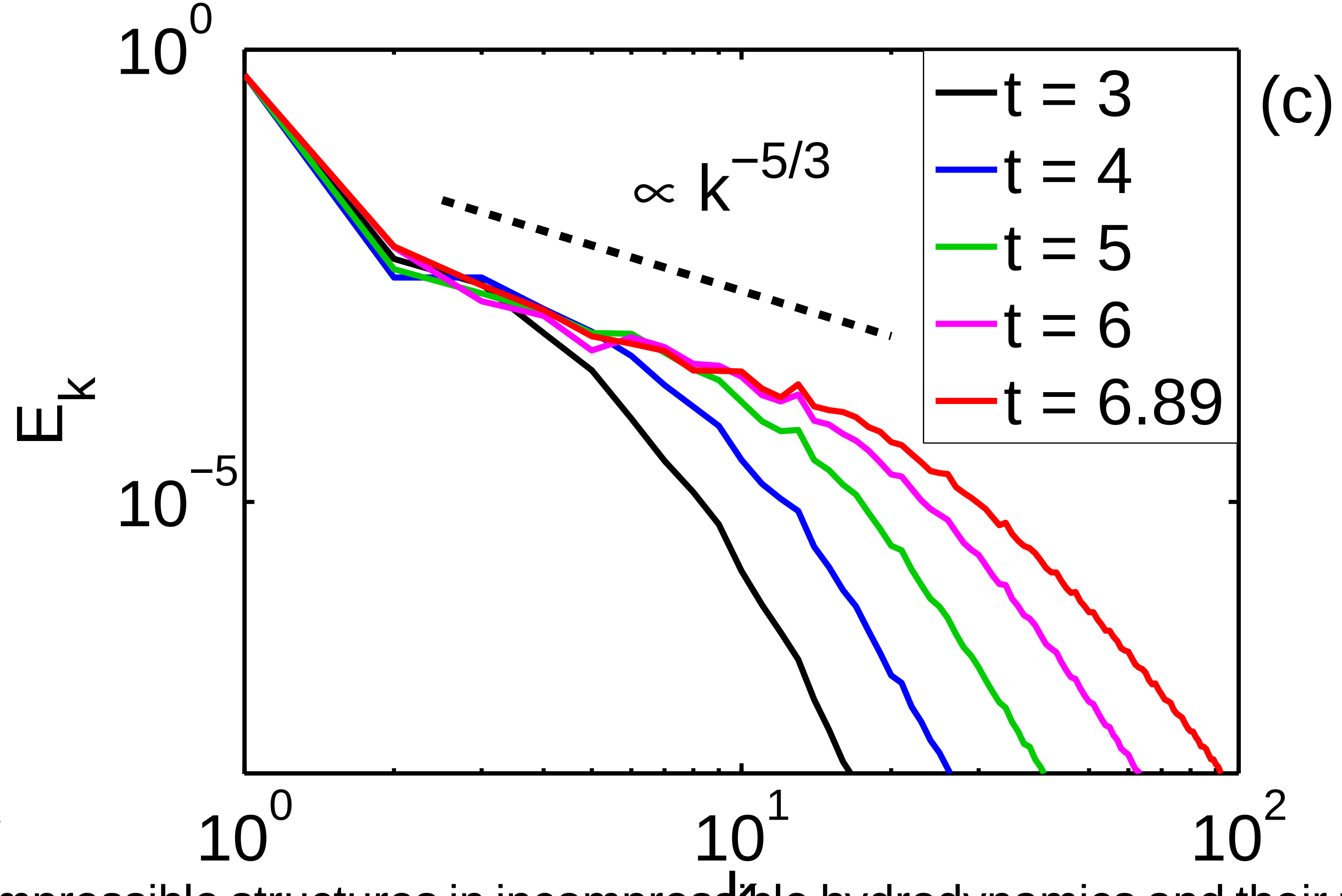

Numerical experiment: spectrum

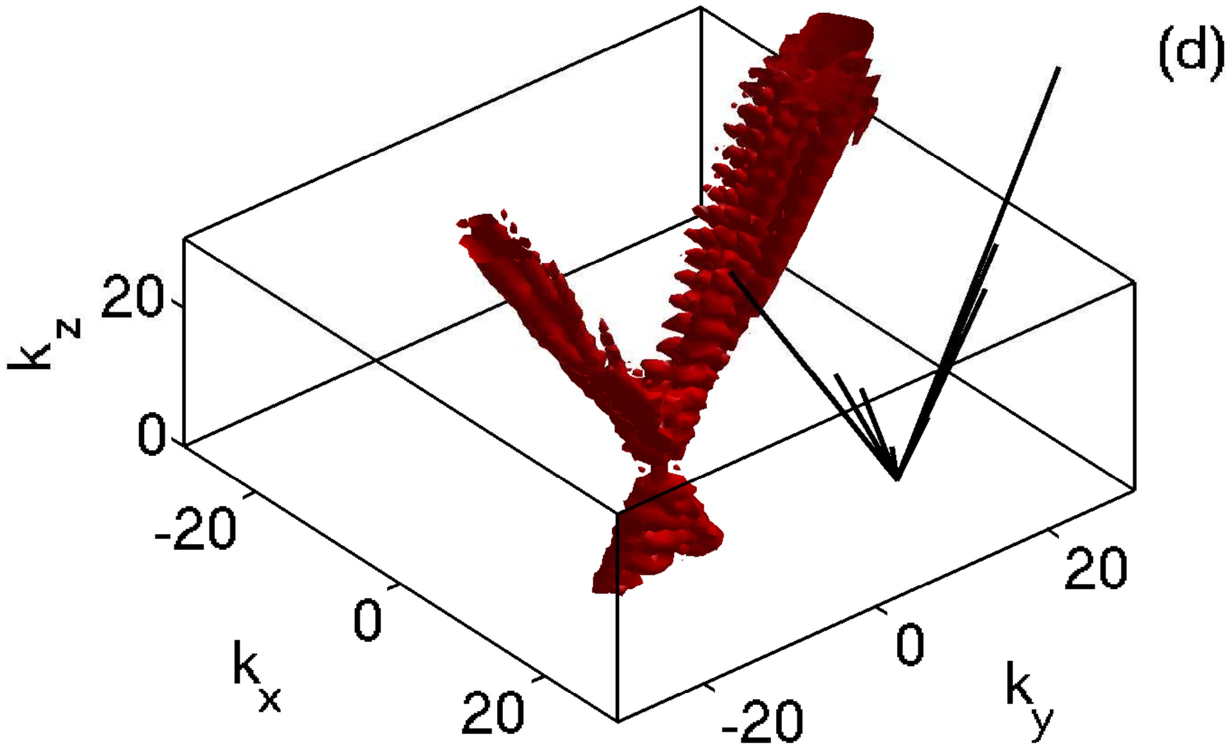

JETS: Isosurface $|\tilde{\omega}(\mathbf{k})| = 0.2$ of the normalized vorticity field in $\mathbf{k}$- space at the final time. Solid lines show maximal $\mathbf{k}$-vectors for all jets (normalized by $1/\ell_1$).

Conclusion of the Ist part

In this talk, based on both VLR and direct numerical integration of 3D Euler, we show:

- At the stage of turbulence arising the spectrum is very far from isotropic (in the inertial interval).
- The main contribution in the spectrum in 3D is connected with appearance of coherent structures of the pancake type which in the turbulent spectrum are responsible for jets with growing in time anisotropy. (First time such structures were observed by M. Brachet, et.al. (1992).)
- The maximal pancake vorticity and its width ℓ are connected by means of the Kolmogorov type relation:

$$\omega_{max} \sim \ell^{-2/3}.$$

Conclusion of the Ist part

- Appearance of the pancake structures is a consequence of compressibility of the vorticity lines as it follows from the vortex line representation (K. & Ruban, 1998, K. 2002). These structures develop in time exponentially.
- Increasing with time number of such structures leads to formation of the Kolmogorov energy spectrum observed numerically in a fully inviscid flow, with no tendency towards finite-time blowup.

References

1. E.A. Kuznetsov, V.P. Ruban, *Hamiltonian dynamics of vortex lines for systems of the hydrodynamic type*, JETP Letters, **67**, 1076-1081 (1998); *Hamiltonian dynamics of vortex and magnetic lines in the hydrodynamic type models*, Phys. Rev E, **61**, 831-841 (2000).
2. E.A. Kuznetsov,*Vortex line representation for flows of ideal and viscous fluids* , JETP Letters, **76**, 346-350 (2002); physics/0209047.
3. D.S. Agafontsev, E.A. Kuznetsov and A.A. Mailybaev, *Development of high vorticity structures in incompressible 3D Euler equations*, Physics of Fluids **27**, 085102 (2015).

References

4. D.S. Agafontsev, E.A. Kuznetsov and A.A. Mailybaev, *Development of high vorticity structures in incompressible 3D Euler equations: influence of initial conditions* JETP Letters **104**, 685Ű689 (2016).

5. D.S. Agafontsev, E.A. Kuznetsov and A.A. Mailybaev, *Asymptotic solution for high vorticity regions in incompressible 3D Euler equations*, J. Fluid Mech. **813**, R1 (1-10) (2017).

6. D.S. Agafontsev, E.A. Kuznetsov and A.A. Mailybaev, Development of high vorticity structures and geometrical properties of the vortex line representation, Phys. Rev. Fluids (submitted) 23 pages (2018); arXiv:1712.09836 [physics.flu-dyn].

2D turbulence: Kraichnan vs Saffman spectra

- Following Kolmogorov (1941), each integral in its own transparency region must provide the corresponding Kolmogorov spectrum.
- For 2D HD turbulence, the energy conservation provides the Kolmogorov spectrum $E_k \sim \epsilon^{2/3} k^{-5/3}$ with energy flux ϵ directed to small k: inverse cascade, Kraichnan (1967).
- The enstrophy conservation provides the Kraichnan spectrum(1967) with the constant enstrophy flux η directed to large k (direct cascade): $E_k \sim \eta^{2/3} k^{-3}$.
- The existence of these two spectra has been confirmed in many numerical experiments simulating 2D turbulence at $Re \gg 1$ when in the corresponding inertial intervals one can use the Euler equations, instead of the NS equations.

2D turbulence: Kraichnan vs Saffman spectra

- (1971) Saffman spectrum: Just after the Kraichnan' paper (1968), in the first numerical experiments (Lilly, 1971) there was observed the emergence of sharp vorticity gradients in the form of quasi-shocks with thicknesses small compared to their length. Based on these observations, Saffman proposed another spectrum $E_k \sim k^{-4}$ (the main contribution comes from isotropically distributed quasi-shocks).
- The Saffman' idea was developed by K., Naulin, Nielsen, & Rasmussen, 2007. If vorticity ω undergoes jumps with widths $\delta \ll L$, the characteristic scale, then the spectrum generated by jumps should be $\sim k^{-3}$. Each jump gives the jet-like distribution with apex angle $\theta \sim (kL)^{-1}$. In a pure isotropic case we arrive at the Saffman spectrum.

2D turbulence: Kraichnan vs Saffman spectra

- **Thus, the Kraichnan-type spectrum generated by quasi-singularities must be anisotropic (symmetry breaking).** That is evidenced by both analytical arguments and numerical experiments in the case of a freely two-dimensional turbulence when anisotropy in turbulence spectra is due to the presence of jets (K., Neilson, Naulin, & Rasmussen, 2007; Kudryavtsev, K., & Sereshchenko, 2013; K. (2004)). In these papers, it was revealed physical mechanism of quasi-shocks formation because of a tendency to breaking.
- Note that this process in a finite time is forbidden according to strong theorems (Wolibner,1933; Yudovich, 1963; Kato,1967).

Tendency to breaking in 2D turbulence

Formation of vorticity quasi-shocks can be understood if within the Euler equation

$$\mathbf{v}_t + (\mathbf{v}\nabla)\mathbf{v} = -\nabla p,$$

we obtain first the Helmholtz equation for vorticity $\omega = \nabla \times \mathbf{v}$,

$$\omega_t + (\mathbf{v}\nabla)\omega = 0,$$

and then consider the divergence-free vector $\mathbf{B} = \text{rot}\,\omega$ (di-vorticity, Kida), where $\mathbf{B}$ obeys the equation

$$\frac{\partial \mathbf{B}}{\partial t} = \text{rot}\,[\mathbf{v} \times \mathbf{B}].$$

This vector field is frozen-in-fluid. It is easily seen also that this vector is tangent to the isoline $\omega(x, y) = \text{const}$.

Tendency to breaking in 2D turbulence

In terms of the substantial derivative Eq. for di-vorticity can be rewritten as

$$\frac{d\mathbf{B}}{dt} = (\mathbf{B}\cdot\nabla)\mathbf{v} \equiv \frac{1}{2}\left[\omega\hat{z}\times\mathbf{B}\right] + \hat{S}\mathbf{B}.$$

The r.h.s. describes the rotation of the vector $\mathbf{B}$ and stretching of the di-vorticity lines where

$$\hat{S}_{ik} = \frac{1}{2}\left(\frac{\partial v_k}{\partial x_i} + \frac{\partial v_i}{\partial x_k}\right)$$

is the stress tensor. The di-vorticity length $|\mathbf{B}|$ will locally increase when

$$\frac{1}{2}\frac{d\mathbf{B}^{\mathbf{2}}}{dt} = (\mathbf{B}\cdot\hat{S}\mathbf{B}) > 0.$$

Tendency to breaking in 2D turbulence

Now let us introduce new Lagrangian trajectories of the divorticity line, given by $\mathbf{v}_n$, as a solution of the following ODEs,

$$\frac{d\mathbf{r}}{dt} = \mathbf{v}_n(\mathbf{r}, t); \quad \mathbf{r}|_{t=0} = \mathbf{a}.$$

Then $\mathbf{B}$ is expressed through the solution/ mapping $\mathbf{r} = \mathbf{r}(\mathbf{a}, t)$ and its Jacobian J (analog of VLR):

$$\mathbf{B}(\mathbf{r}, t) = \frac{(\mathbf{B}_0(\mathbf{a}) \cdot \nabla_a)\mathbf{r}(\mathbf{a}, t)}{J}$$

where the initial $\mathbf{B_0}$ has a meaning of the Cauchy invariant. J is not fixed, i.e., the mapping is compressible, that is a reason of sharp gradients appearance in 2D Euler (KNNR). The quantity $n = J^{-1}$ plays the role of divortex lines density.

$$n_t + \mathrm{div}_r(n\mathbf{v}_n) = 0, \ \ \mathrm{div}_r \mathbf{v}_n \neq 0.$$

Numerical approach: decay turbulence

- To support the above arguments and reveal the direct connection between the formation of the sharp vorticity gradients and the tail of the energy spectrum first we performed numerical experiments of the evolution of decaying 2D turbulence.
- We solve numerically the vorticity equation with hyperviscosity

$$\frac{d\omega}{dt} = (-1)^{n+1}\mu_n \nabla^{2n}\omega, \ \ \mu_n = 10^{-20}\left(\frac{2048}{N}\right)^{2n}, \quad n = 3$$

in a double periodic domain whose size is taken to be unity. The simulations conserve the total energy and enstrophy with a relative error smaller than 10^{-9}.

Numerical approach: decay turbulence

- We use pseudospectral Fourier method and the 3rd order Runge–Kutta / Crank–Nicolson scheme. The FFTW library is used for computing the discrete Fast Fourier Transform.
- The computations have been performed on both the multiprocessor cluster (with MPI parallelization, up to 128 processors have been used) and the GPU cluster (using NVIDIA CUDA technology) at the Novosibirsk State University Computational Center.
- Spatial resolution was up to 8192×8192. The time scale corresponds to inverse maximal value of vorticity, ω_0^{-1}.

Numerical experiments for 2D decay turbulence

Initial distribution of ω. Distribution of vorticity at $t = 100$.

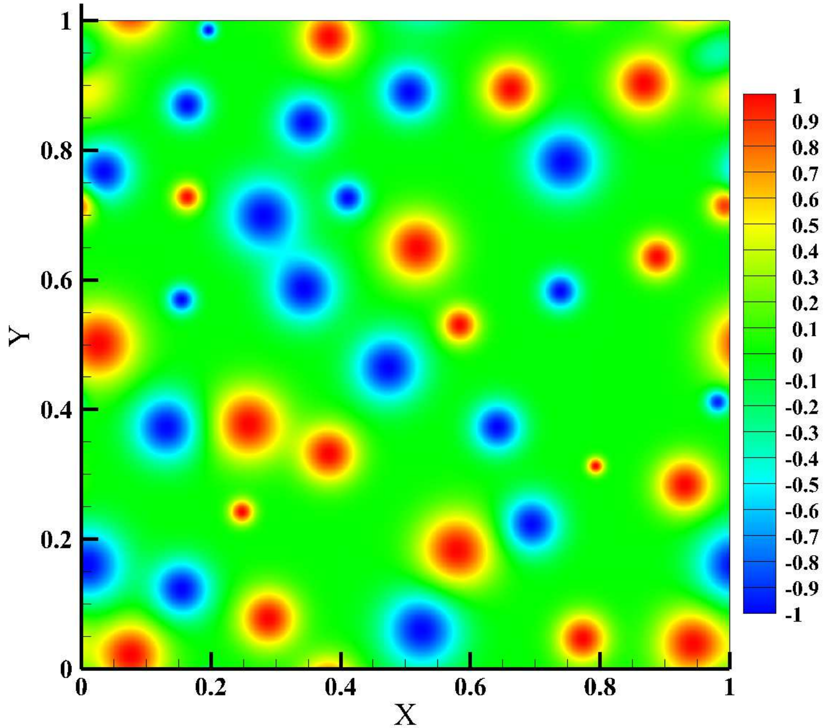

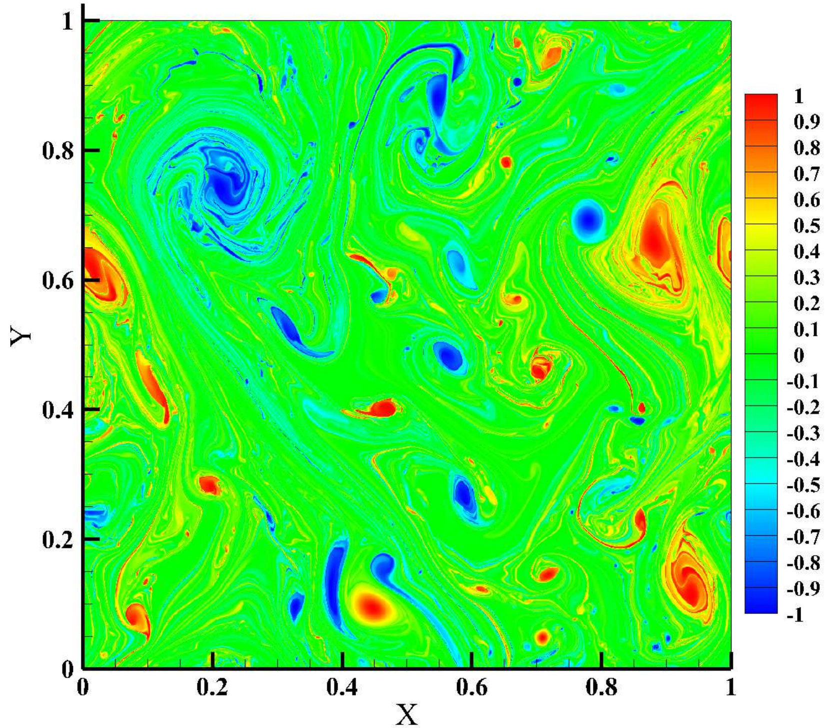

Vortices of both signs $N = 20$ with the Gaussian profile, a random radius and the unit maximum ω are randomly spaced within the domain with the zero total circulation.

Numerical experiments for 2D decay turbulence

Compensated energy spectrum at different times $k^3E(k)$

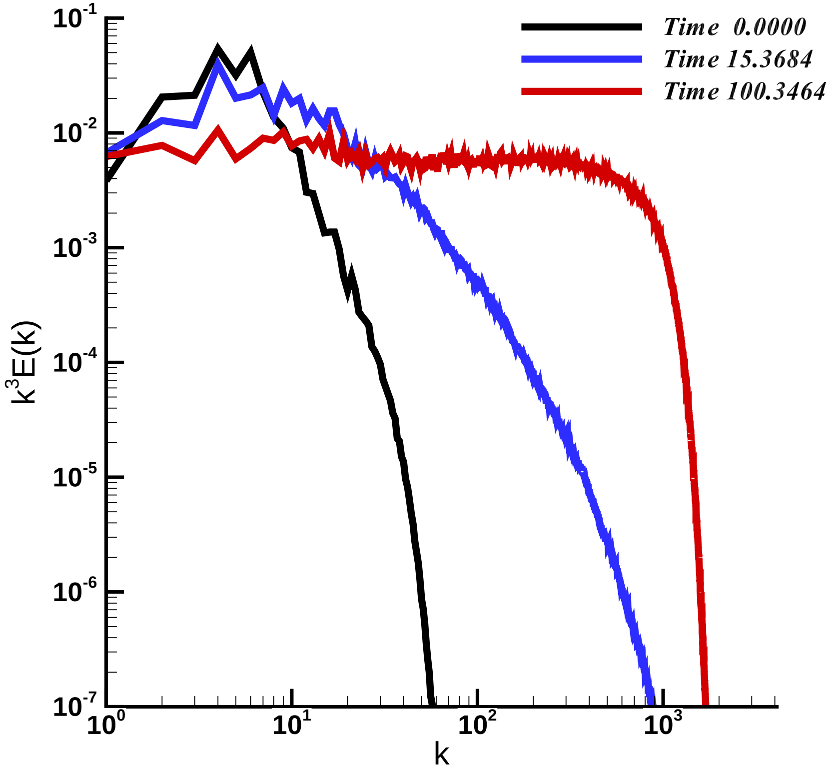

Numerical experiments for 2D decay turbulence

Distribution of $|\mathbf{B}|$ at $t = 100$

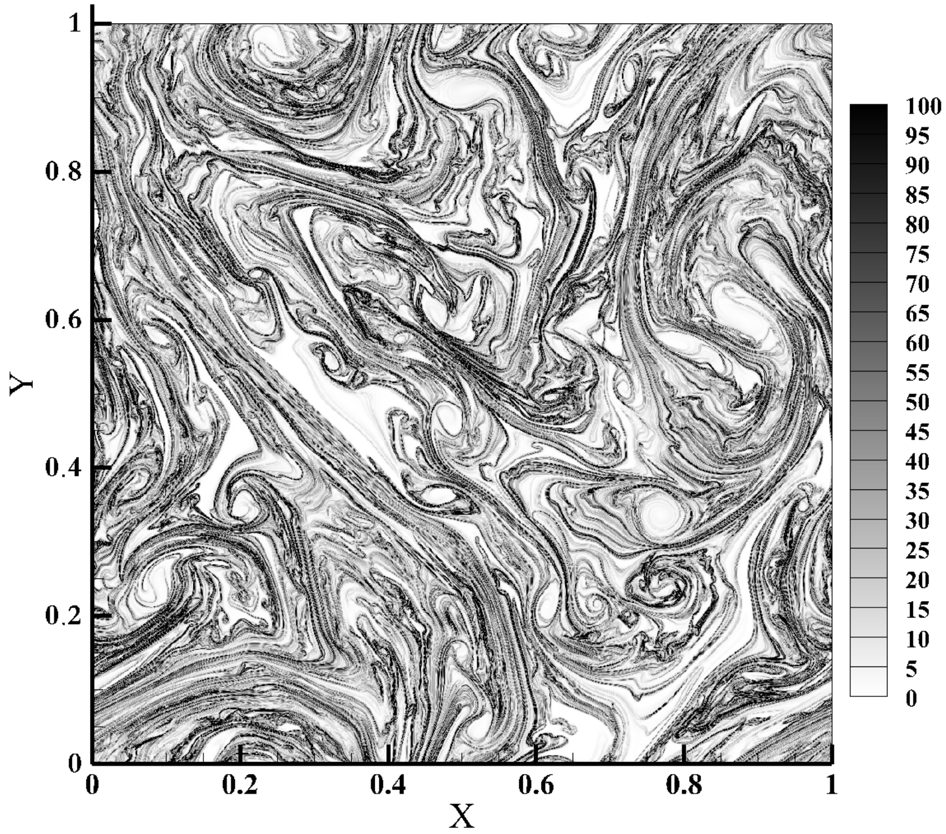

Numerical experiments for 2D decay turbulence

Dependence of B on x at $t = 75$ ($y = 0$).

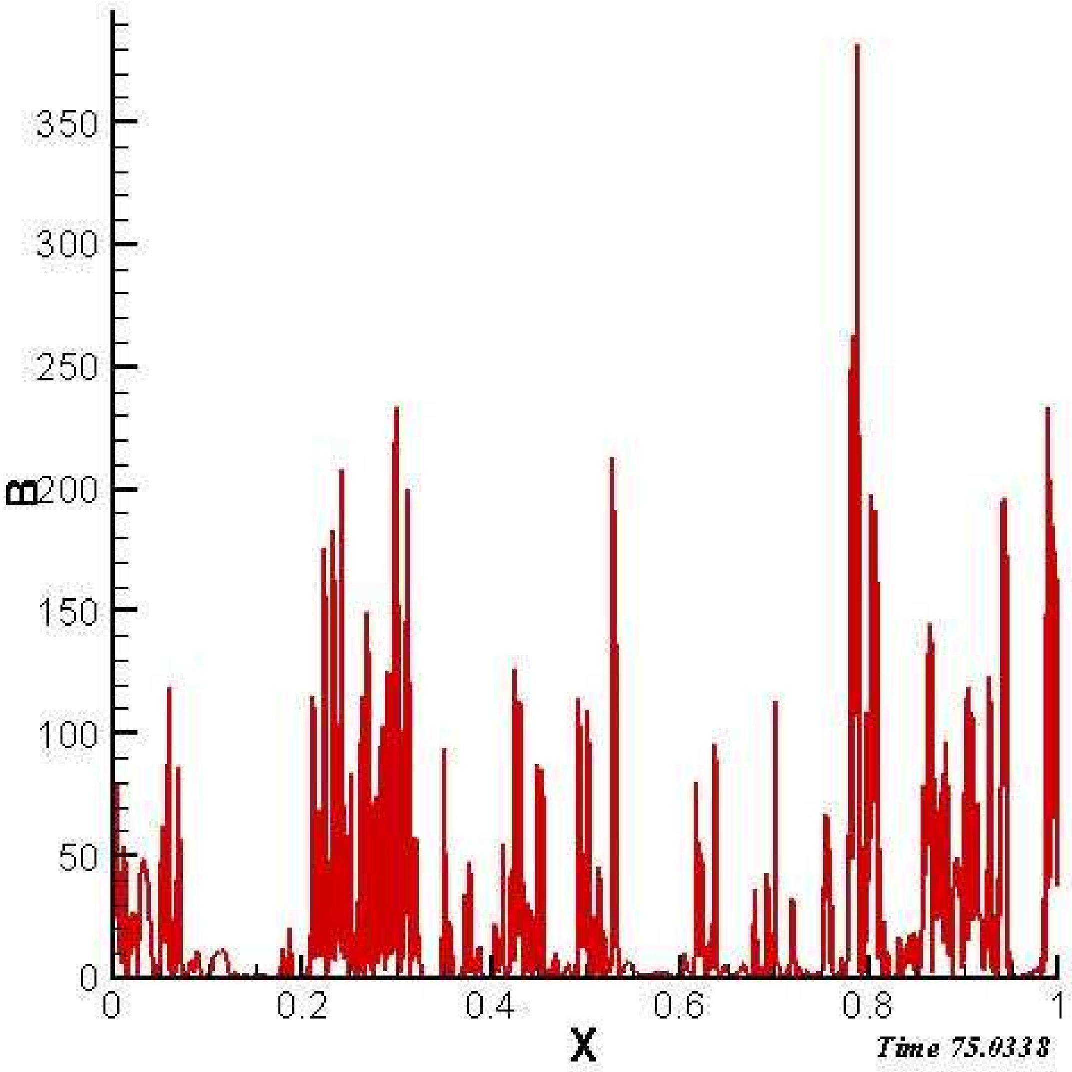

Numerical experiments for 2D decay turbulence

Growth of maximum of di-vorticity (logarithmic scale, the straight line corresponds to the exponential growth)

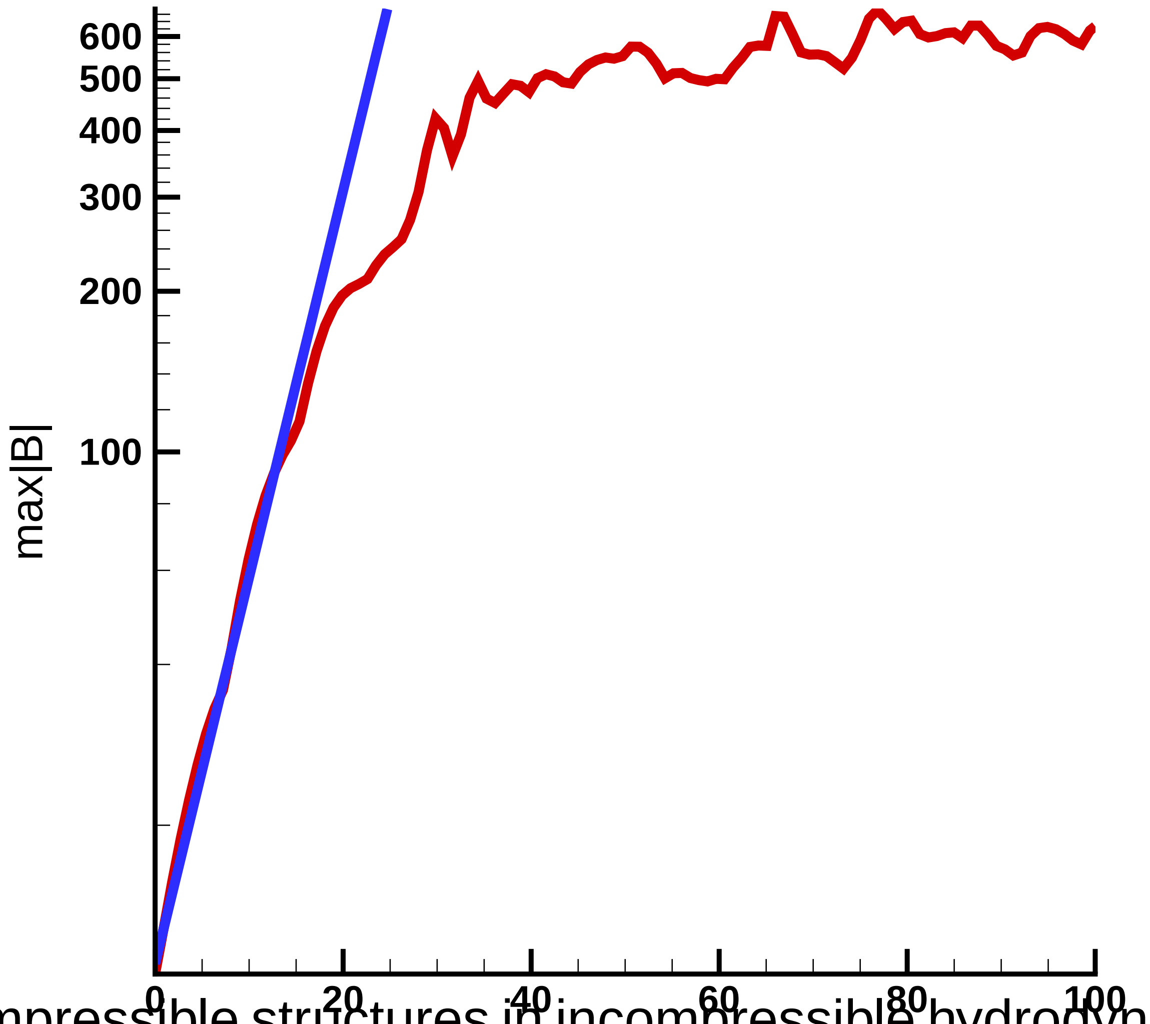

Numerical experiments for 2D decay turbulence

2D energy spectrum $k^4\epsilon(k_x, k_y)$ at $t = 100$

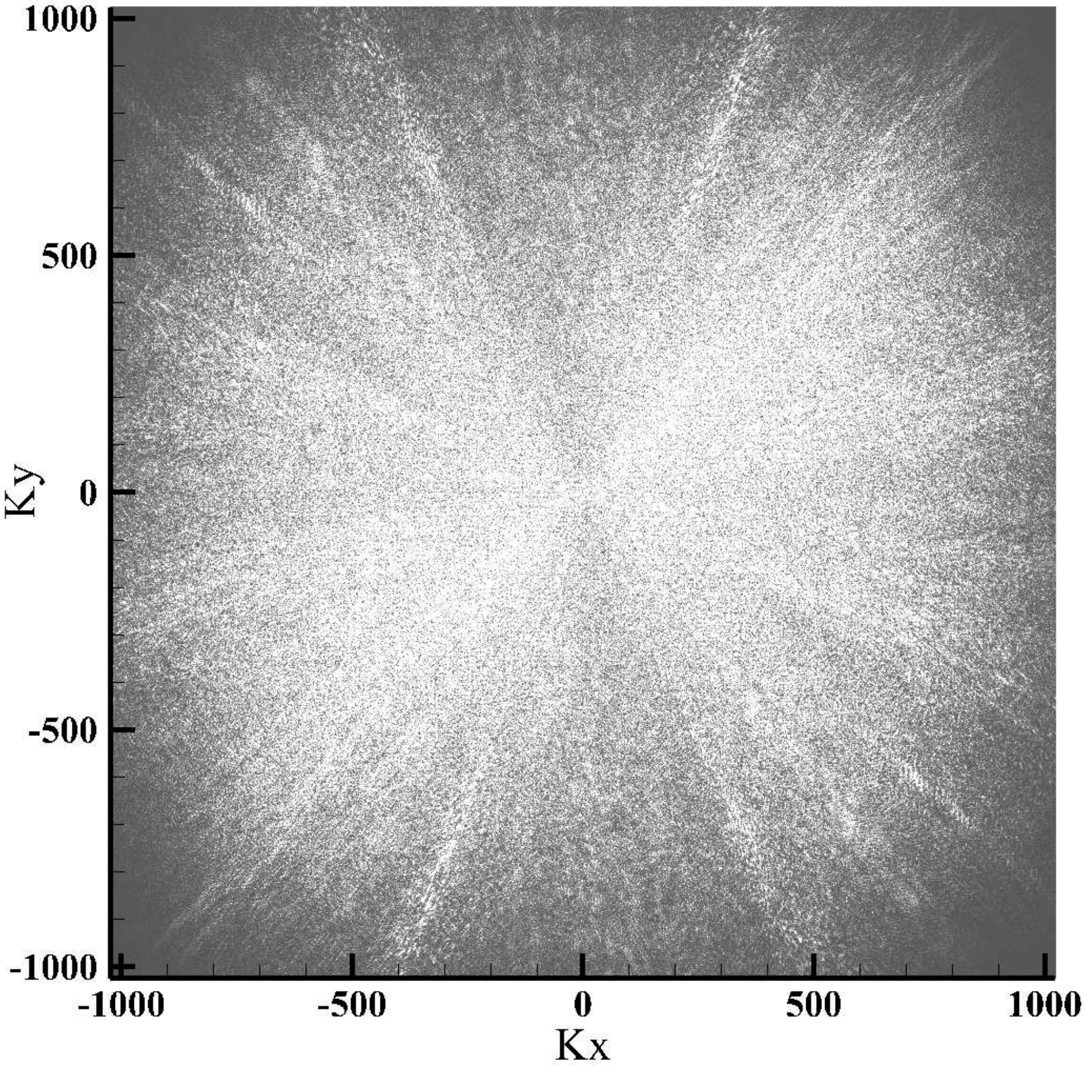

Numerical experiments for 2D decay turbulence

Filtered compensated spectra $k^3\widetilde{E}(k)$ for different threshold values B_0 ($t = 100$)

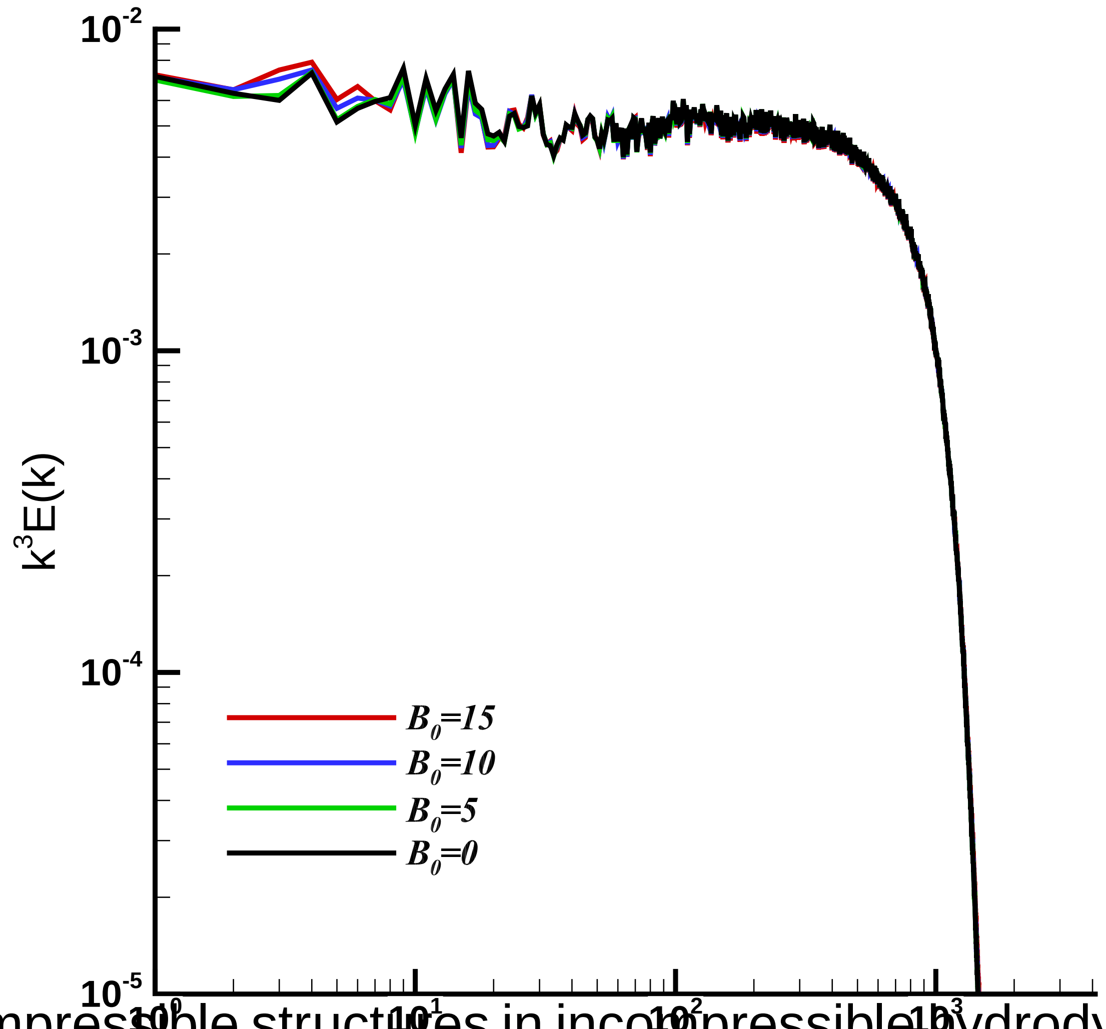

Numerical experiments for 2D decay turbulence

The velocity structure functions

$$S_n(R) = \left\langle \left[(\mathbf{v}(\mathbf{r}') - \mathbf{v}(\mathbf{r})) \cdot \frac{\mathbf{r}'-\mathbf{r}}{r'-r} \right]^n \right\rangle \sim R^{\zeta_n}.$$

Power law exponents ζ_n (local) as functions of R.

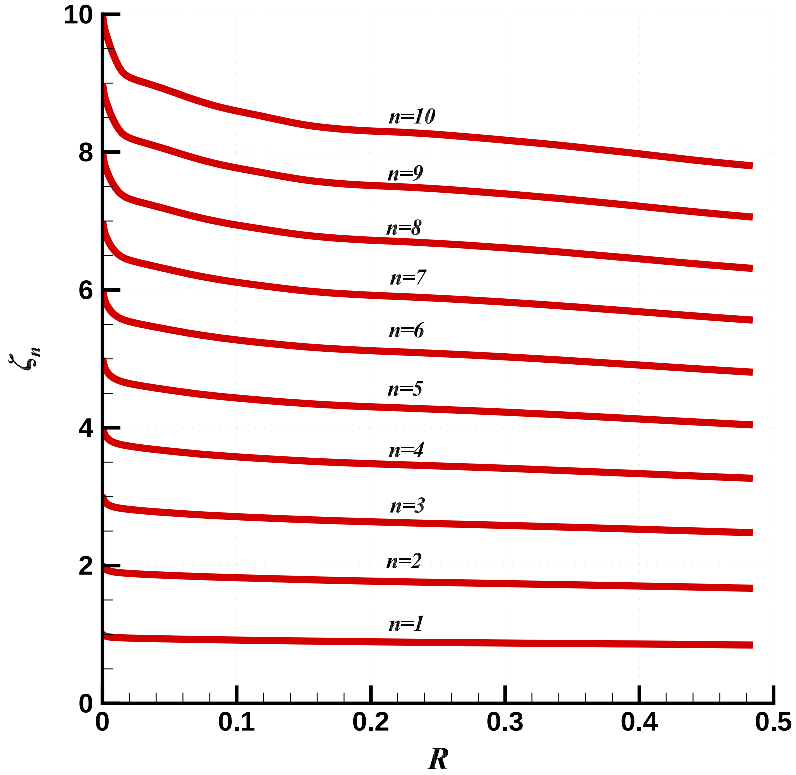

Numerical experiments for 2D decay turbulence

Correlation function $D(R) = \langle \delta u_{\parallel} (\delta\omega)^2 \rangle$.

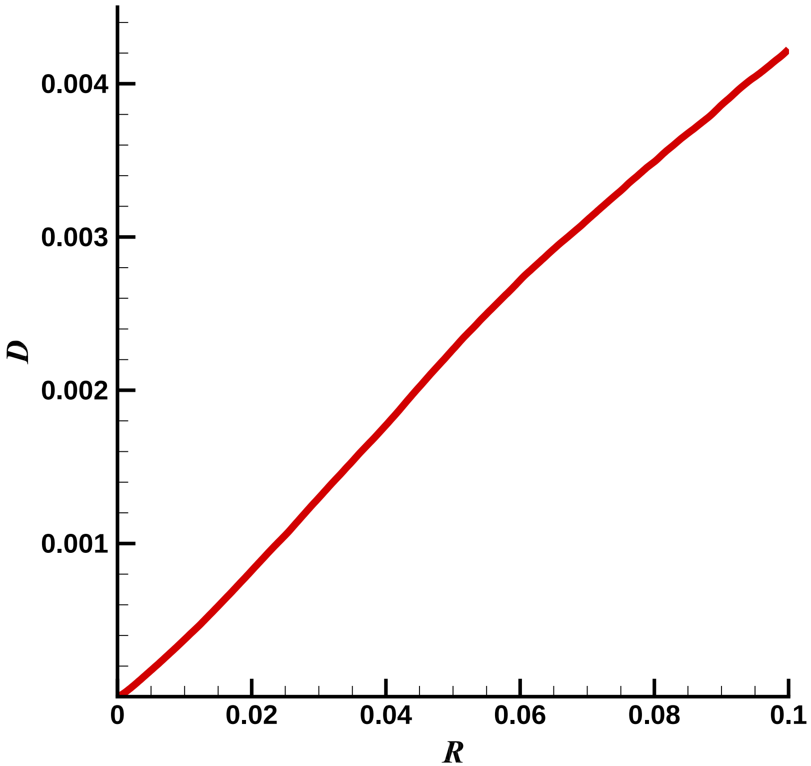

2D turbulence with pumping and viscous-type damping

We consider the two-dimensional Navier-Stokes equation for an incompressible flow in the vorticity formulation,

$$\frac{\partial\omega}{\partial t} + (\mathbf{u}\nabla)\omega = (\hat{\Gamma} + \hat{\gamma})\omega \qquad \text{with} \qquad \text{div}\,\mathbf{u} = 0,$$

where the Fourier transforms of $\hat{\Gamma}$

$$\begin{aligned} \Gamma_k &= A\frac{(b^2-k^2)(k^2-a^2)}{k^2} \quad \text{at} \quad 0 \le k \le b, \\ \Gamma_k &= 0 \quad \text{at} \quad k > b. \end{aligned}$$

and $\hat{\gamma}$ was taken in the viscous-type form with

$$\begin{aligned} \gamma_k &= 0 \quad \text{at} \quad k \le k_c, \\ \gamma_k &= -\nu(k-k_c)^2 \quad \text{at} \quad k > k_c. \end{aligned}$$

2D turbulence with pumping and damping

Time evolution of total energy E and total enstrophy H

($A = 0.004,\ a = 3,\ b = 6,\ \nu = 1.5,\ k_c = 0.6k_{max}$)

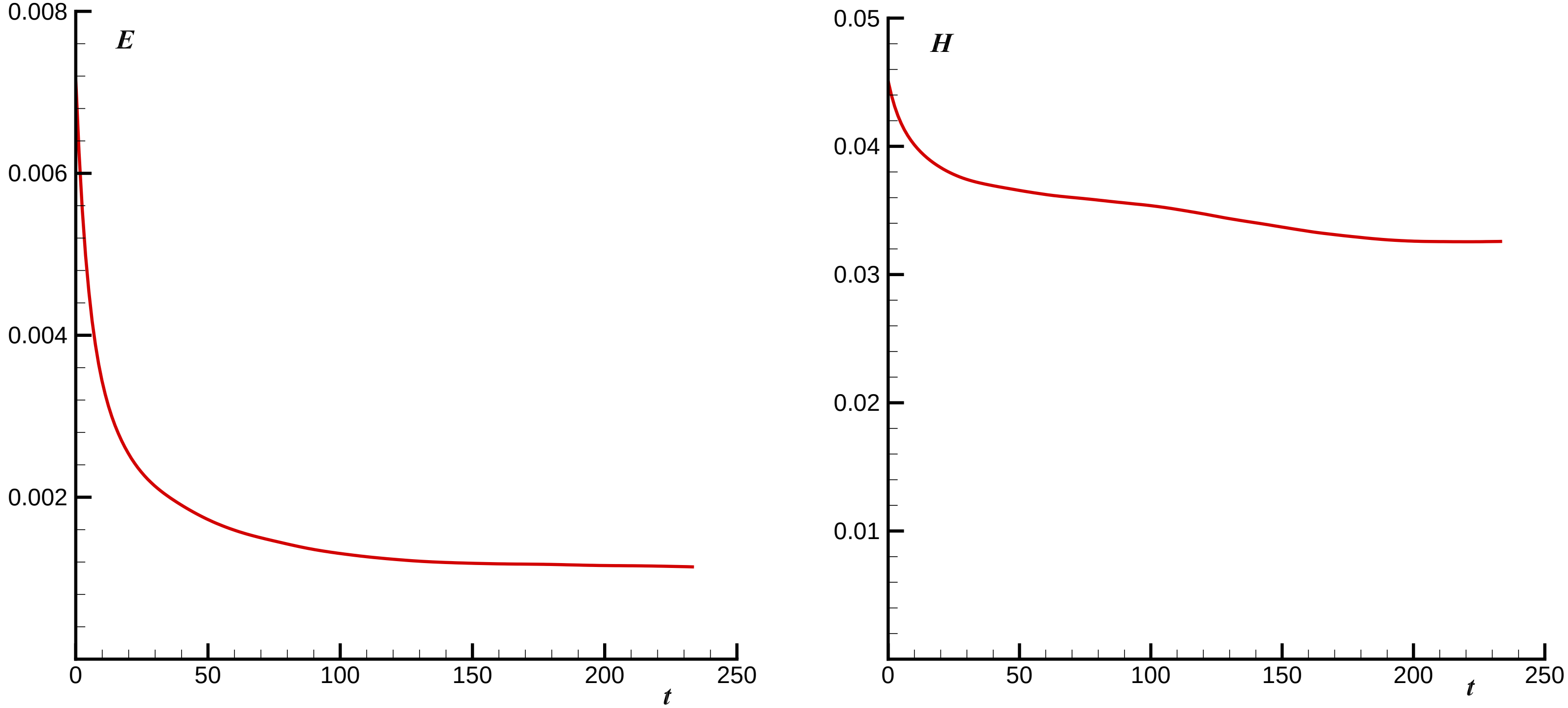

2D turbulence with pumping and damping

Energy spectrum $E(k)$ at different instants of time

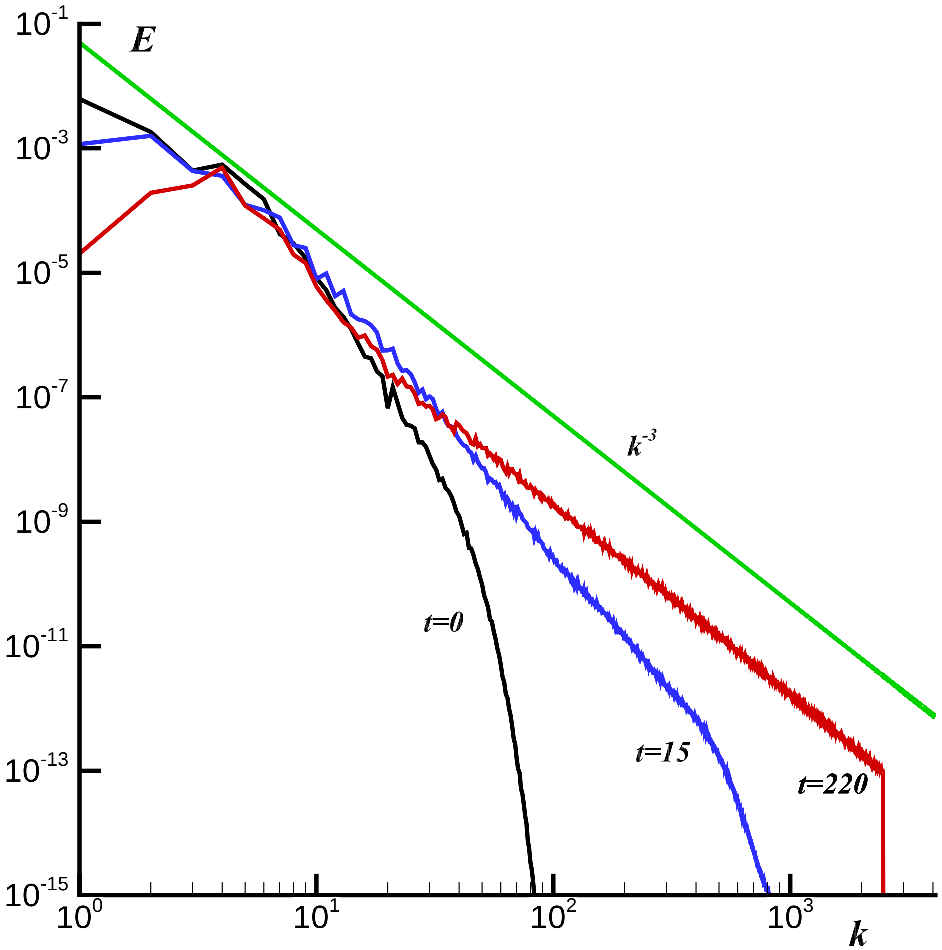

In the «steady» state $E_k = C_K \eta^{2/3} k^{-3}$ with $C_K \simeq 1.3$.

2D turbulence with pumping and damping

Vorticity distributions at $t = 100, 220$

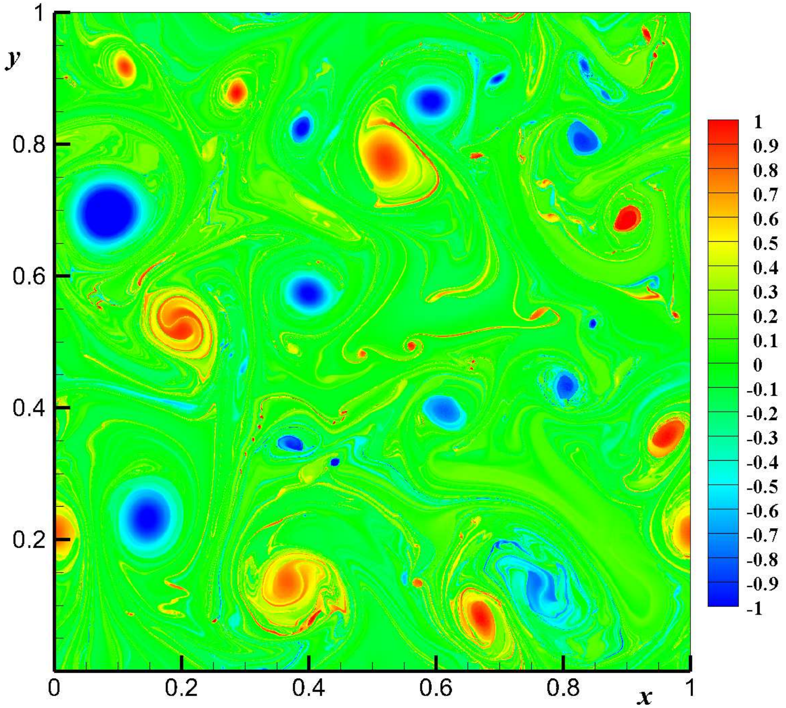

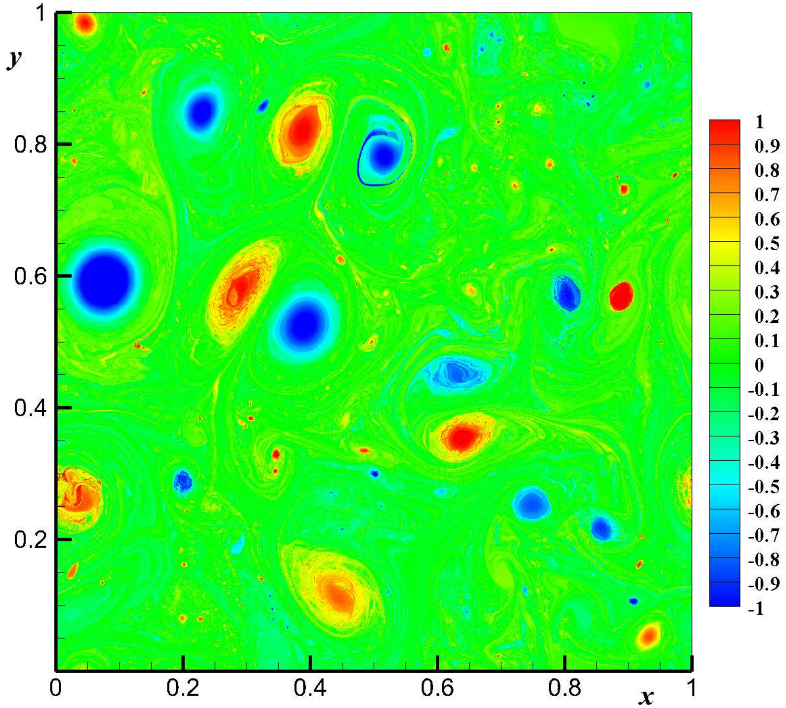

2D turbulence with pumping and damping

Distribution of $|\mathbf{B}|$ at $t = 100, 220$

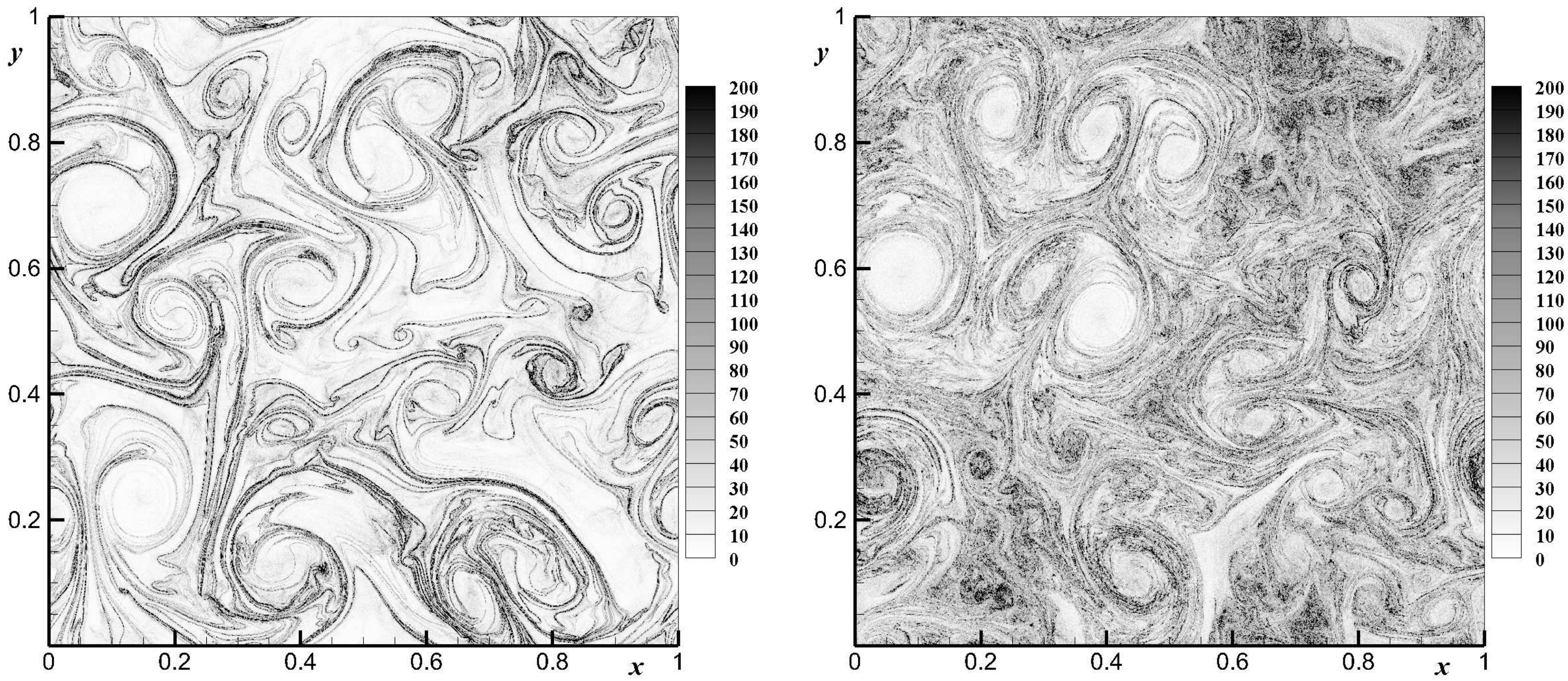

2D turbulence with pumping and damping

Distribution of $|\mathbf{B}|$ along line $y = 0.5$ at $t = 100, 220$.

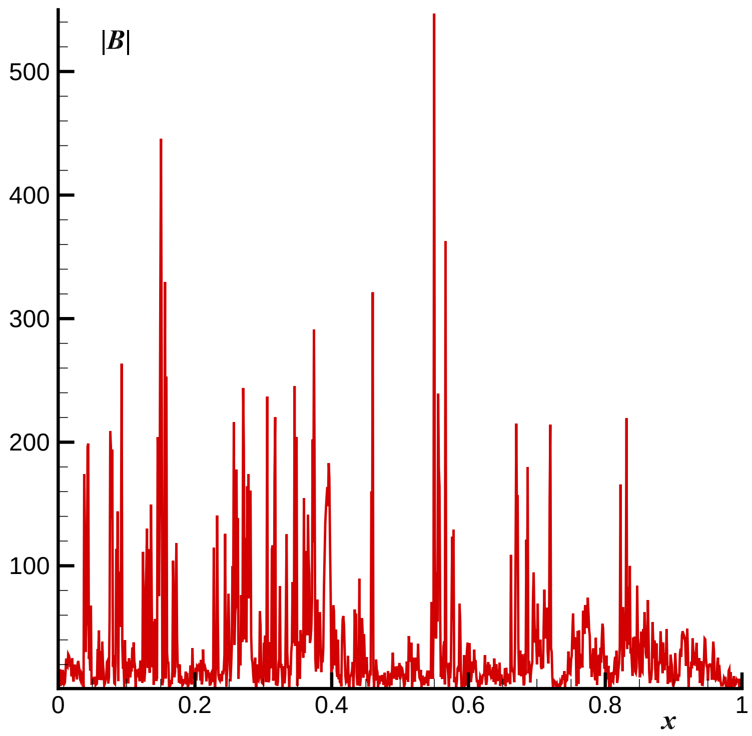

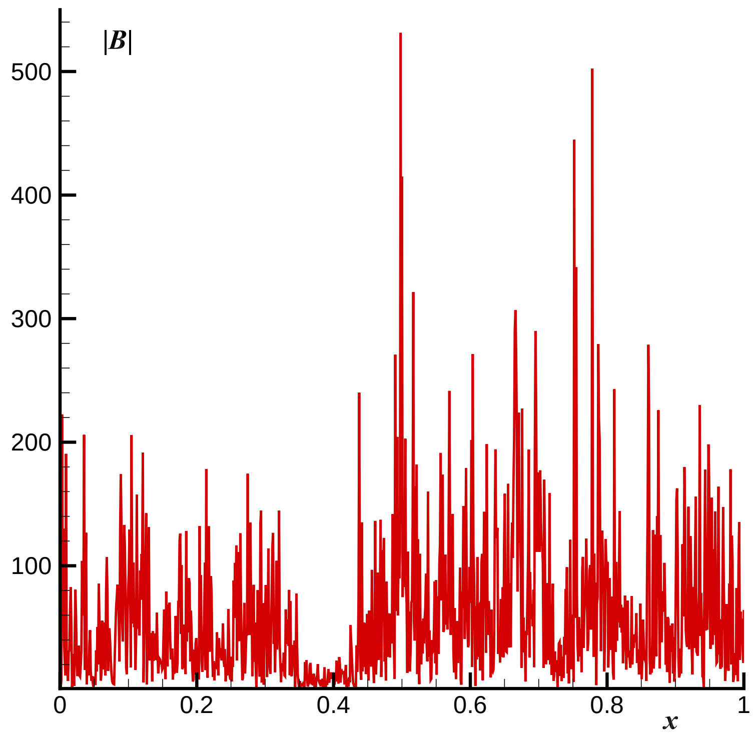

2D turbulence with pumping and damping

2D compensated spectrum $k^4\epsilon(k_x, k_y)$ at $t = 220$

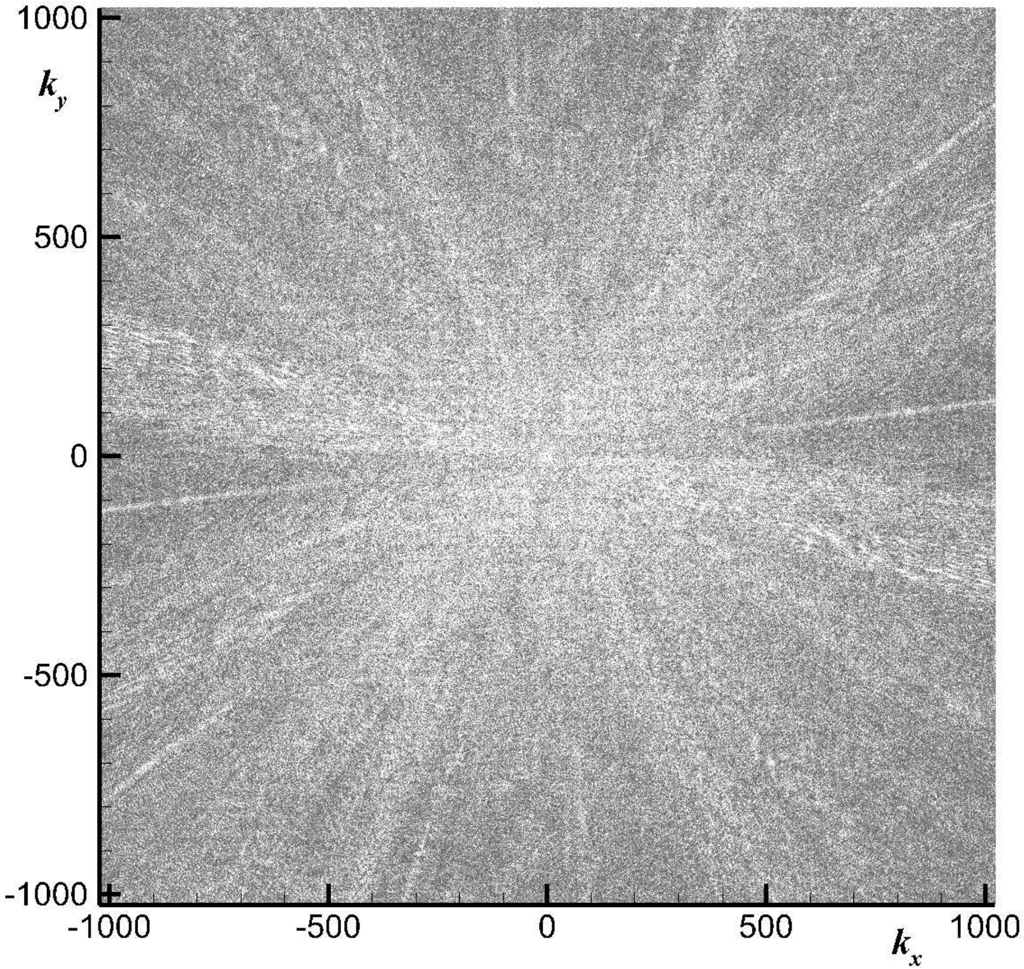

2D turbulence with pumping and damping

Dependence of $S_3^{(L)}$ as function of R at different angles.

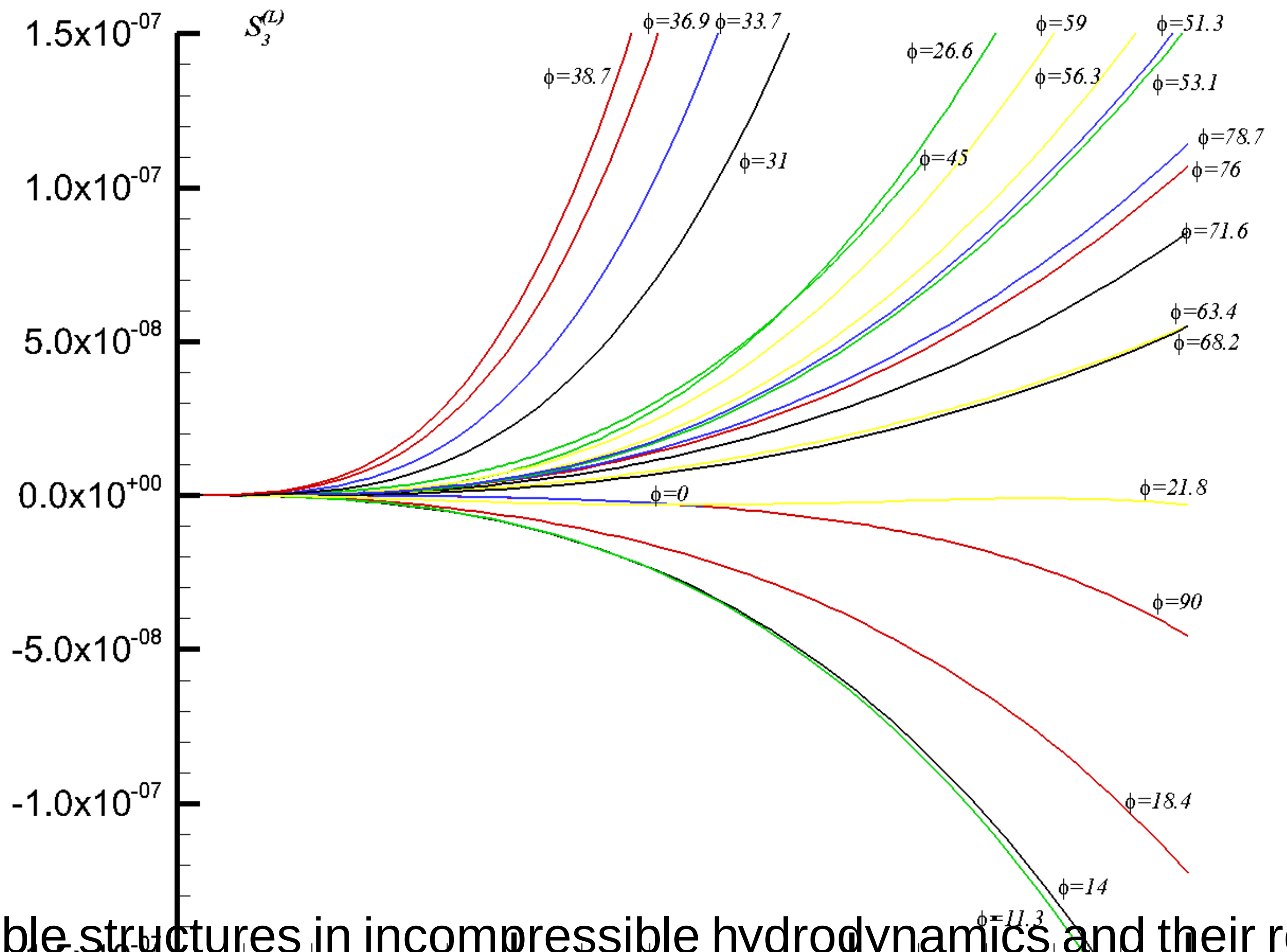

2D turbulence with pumping and damping, grid 16384^2

Distribution of $|B|$ at $t = 150, 250, 450$,

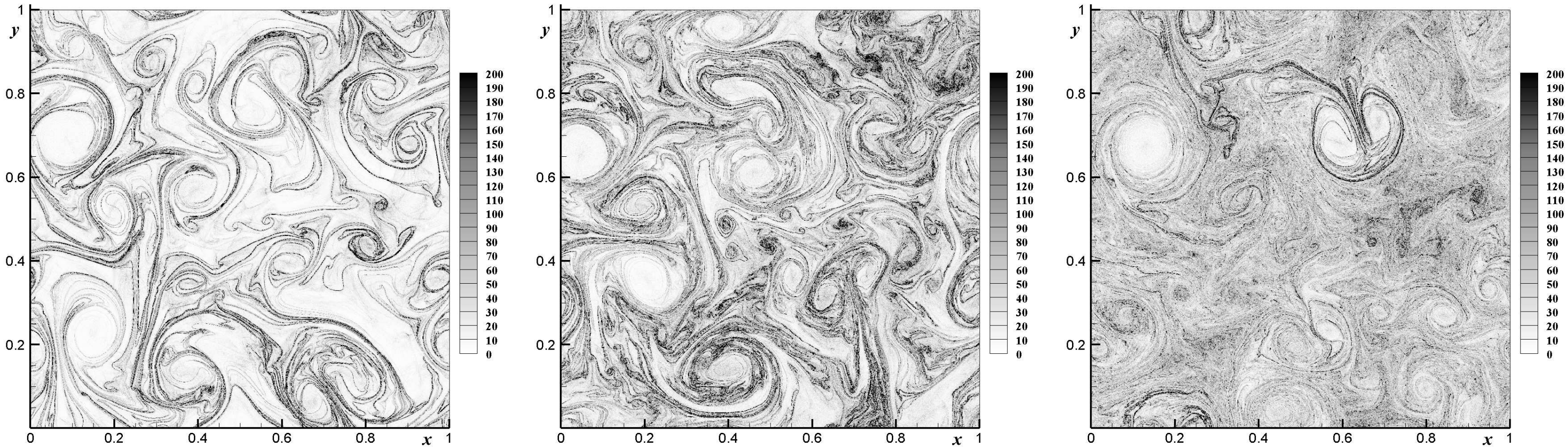

2D turbulence with pumping and damping, grid 16384^2

Spectrum density of the energy $\epsilon(\mathbf{k})$, normalized to k^{-4} at $t = 150, 250, 450$

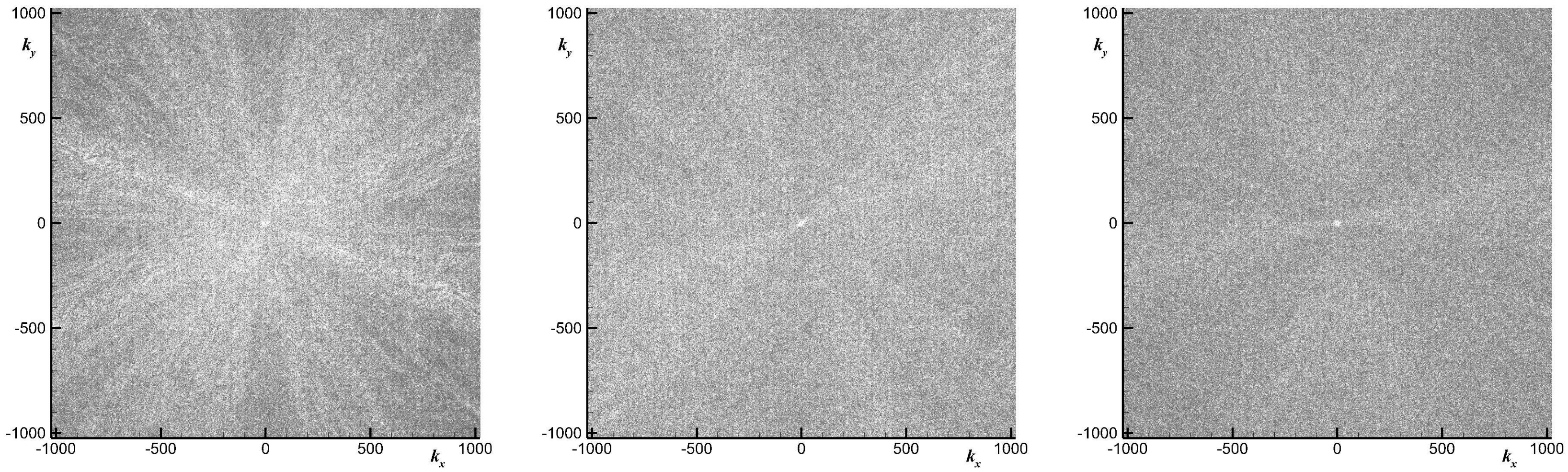

2D turbulence with pumping and damping, grid 16384^2

Dependencies of $\epsilon(\mathbf{k})k^4$ before averaging (a) and averaging value of $\epsilon(\bar{\mathbf{k}})k^4$ in the surrounding $\Delta k = 100$ (b) on k for angle $\phi = 45^\circ$ at $t = 150$.

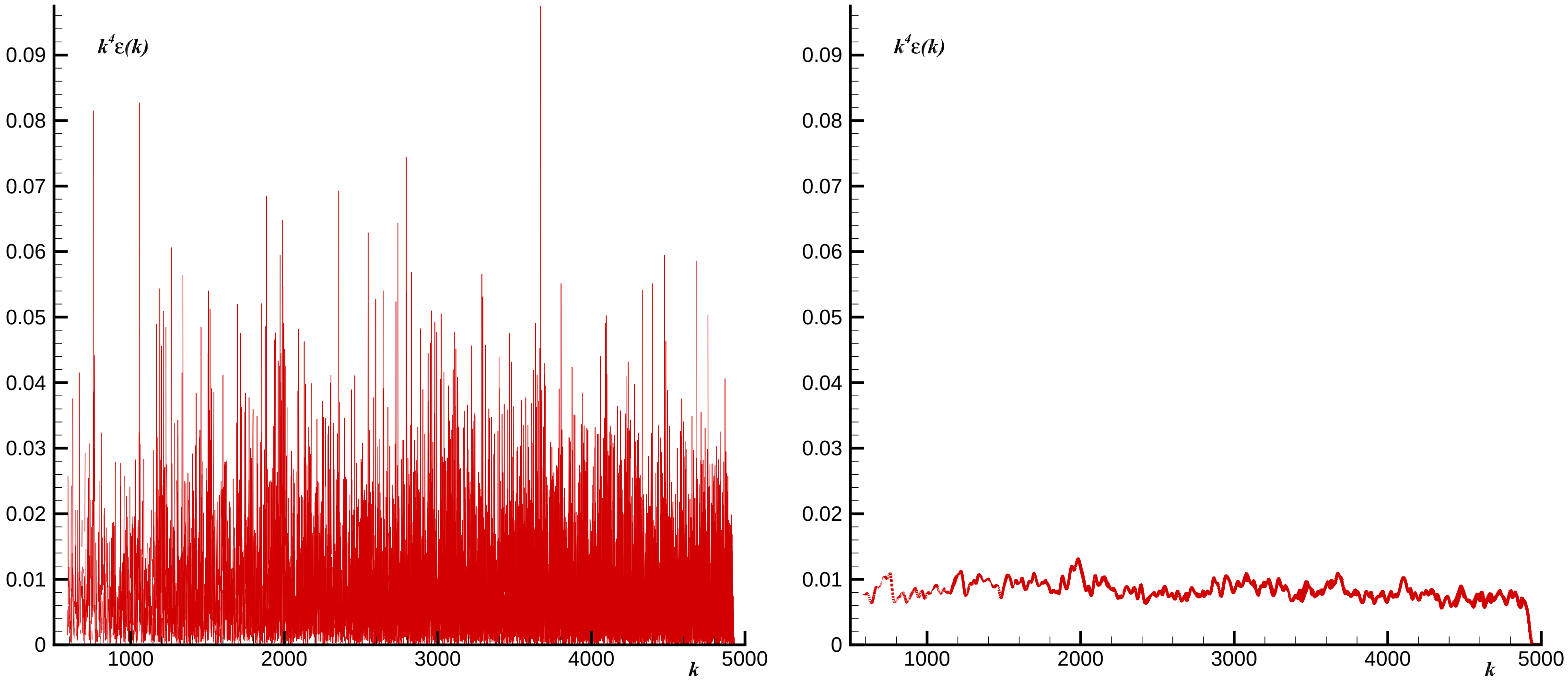

2D turbulence with pumping and damping, grid 16384^2

Time evolution of the enstrophy flux η.

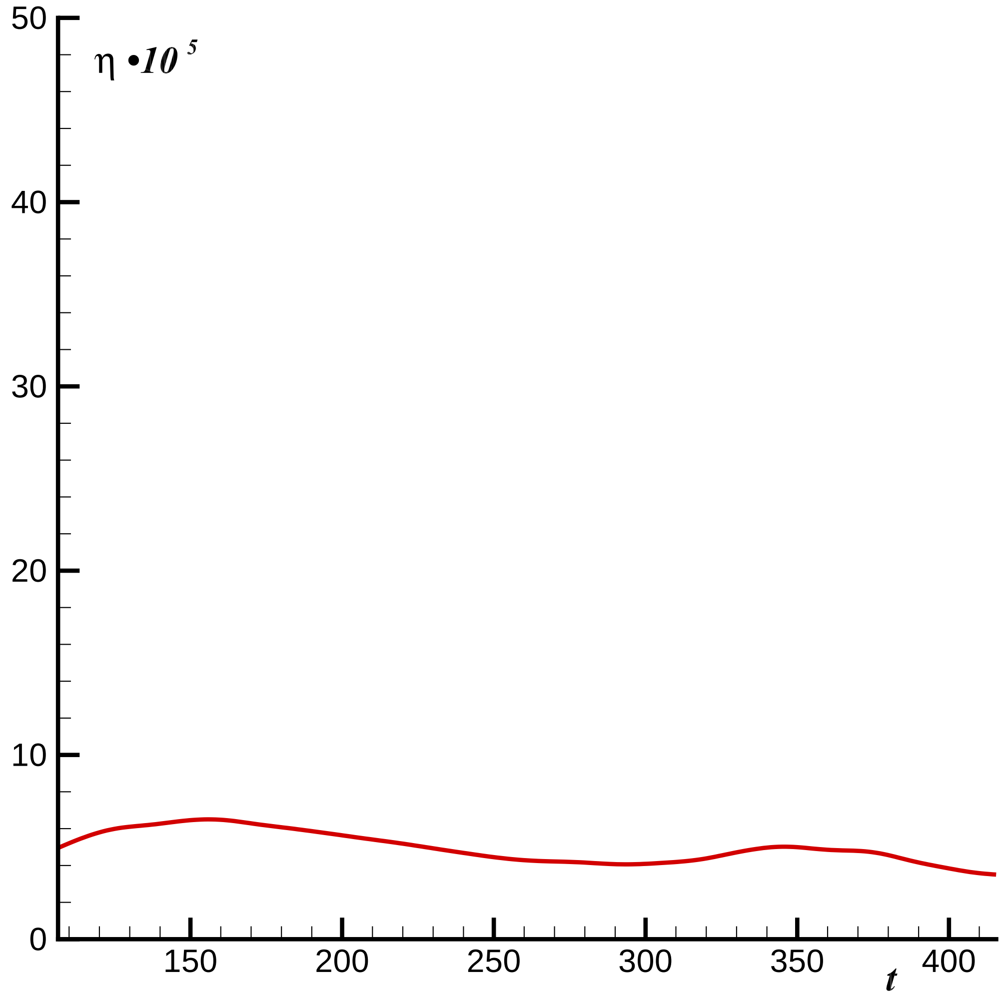

2D turbulence with pumping and damping, grid 16384^2

Time evolutions of the total energy E and total enstrophy H.

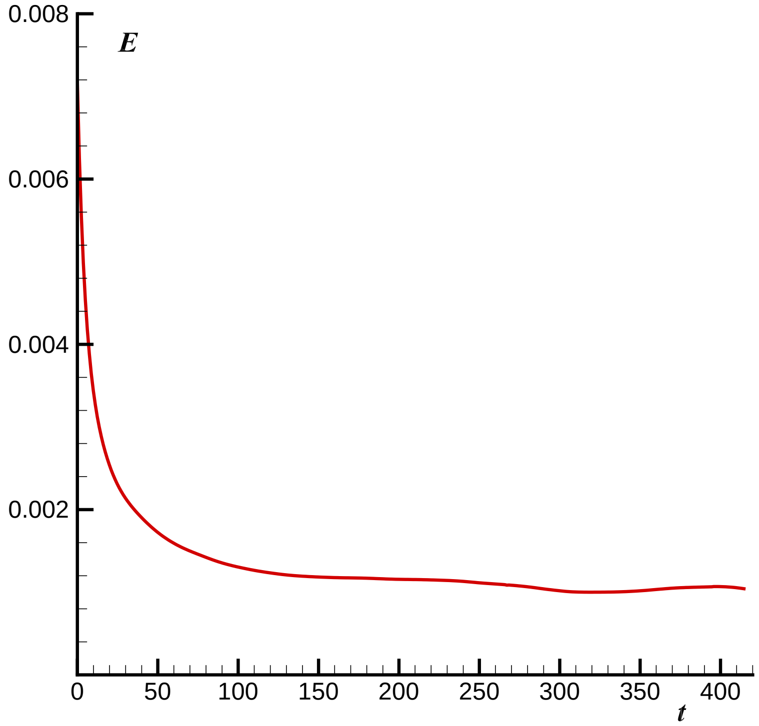

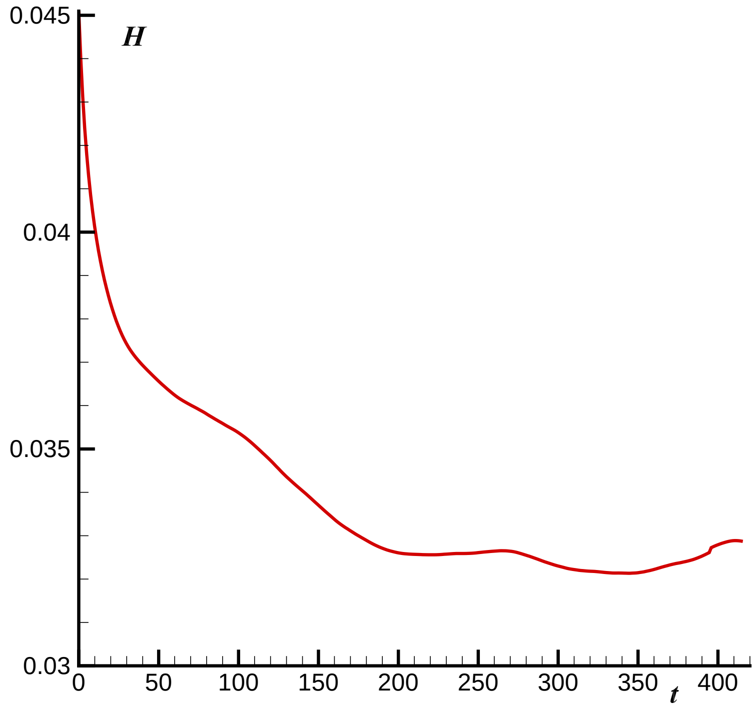

2D turbulence with pumping and damping, grid 16384^2

Probability distribution function of vorticity P at $t = 450$.

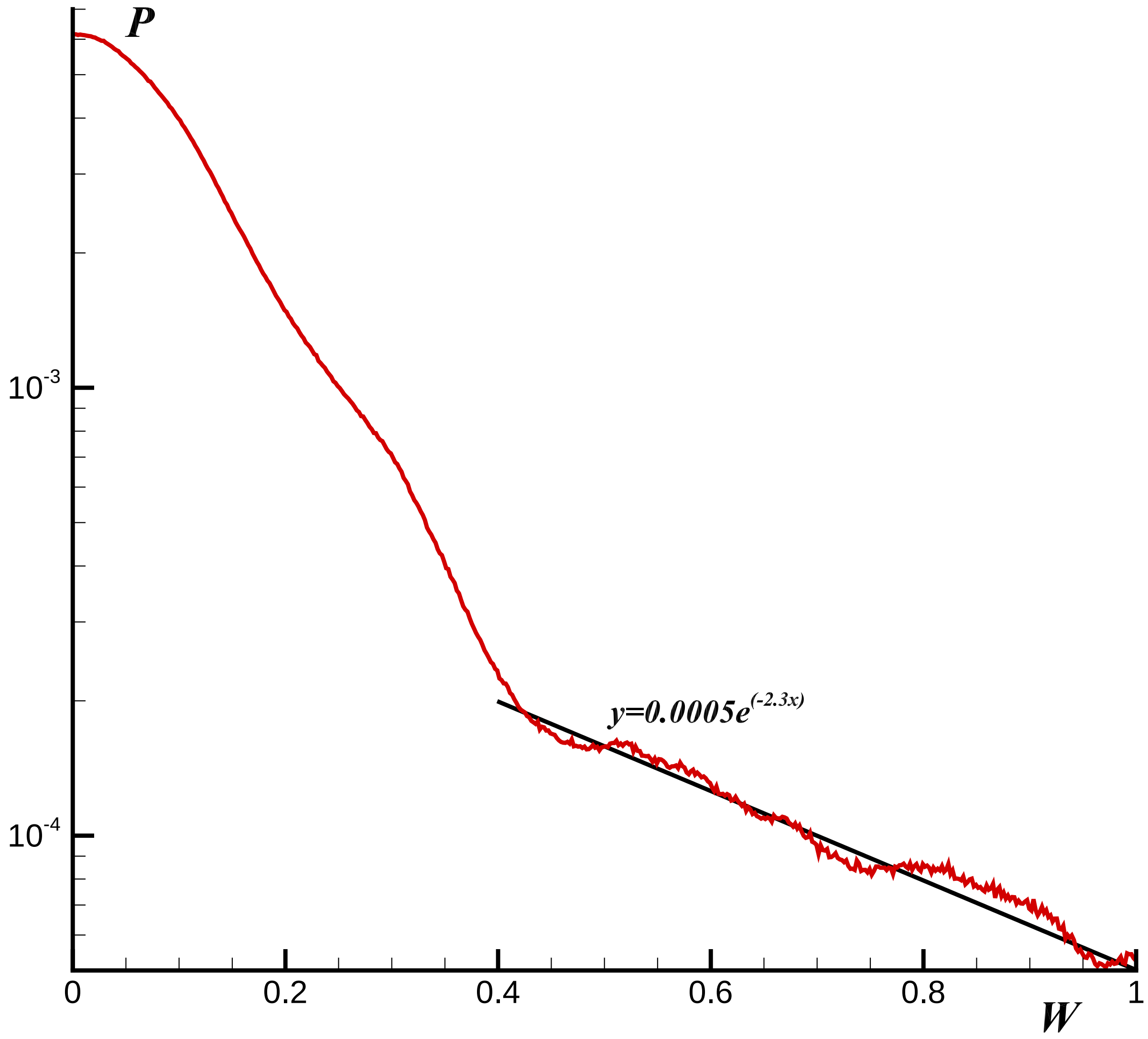

2D turbulence with pumping and damping, grid 16384^2

Probability distribution function of di-vorticity P at $t = 450$.

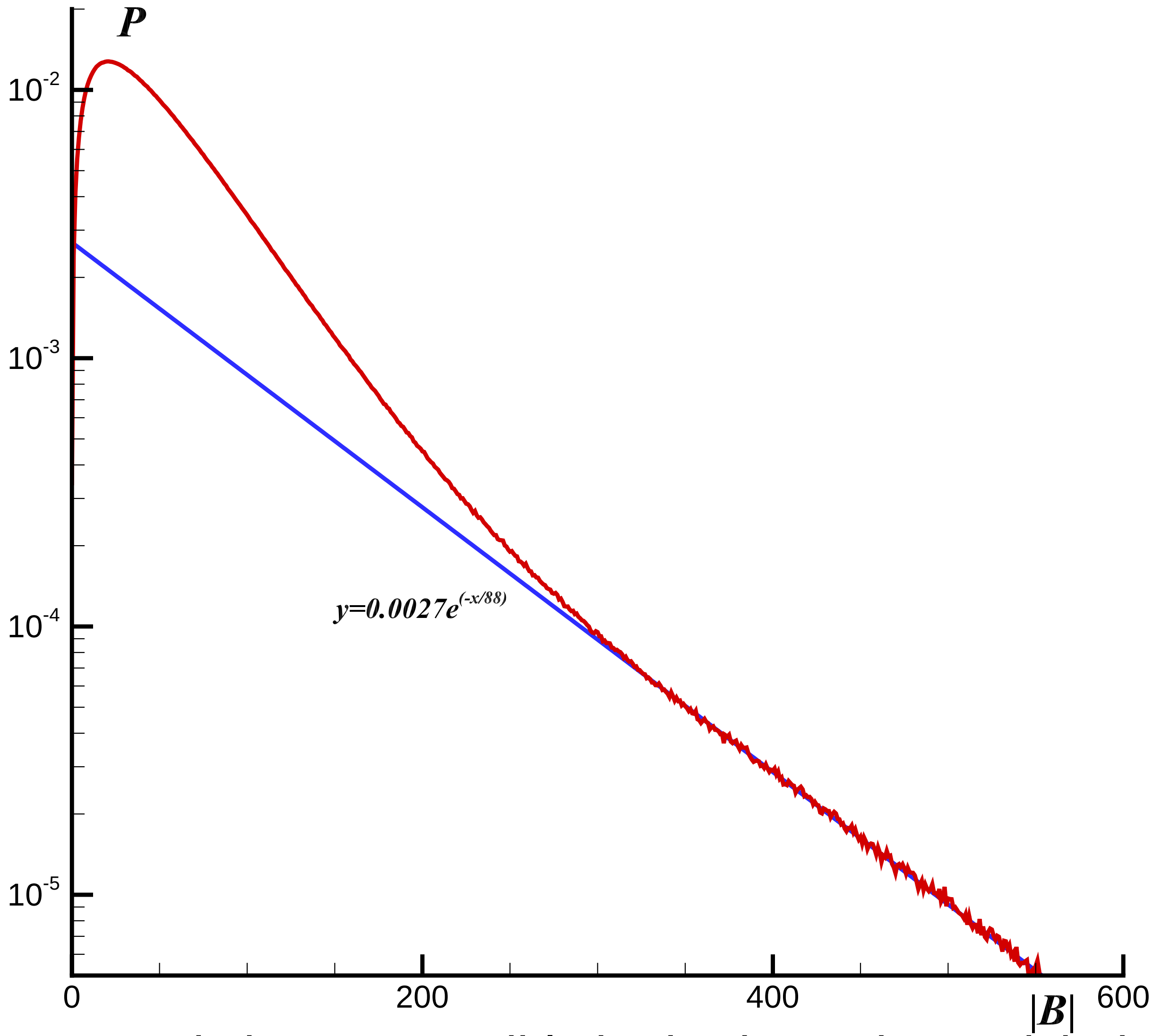

Conclusion of the second part

- For the 2D freely-decaying isotropic turbulence we demonstrated the formation of the vorticity quasi-shocks is responsible for the Kraichnan-type spectrum with the k^{-3} dependence at each angle.
- We have showed that in the presence of both pumping and damping in the direct cascade the power-law dependence on wave number k in the Kraichnan-type spectrum of turbulence is formed by the vorticity quasi-shocks and this process is the fastest one. Its characteristic time is of order of the inverse pumping growth rate $\tau \sim \Gamma_{max}^{-1}$.

Conclusion of the second part

- In the next much slower stage, the structure of quasi-shocks lines becomes complicated. The distances between quasi-shocks lines are reduced, and the spectrum becomes more isotropic. The isotropization time is estimated as 10τ.
- The probability distribution function of vorticity at these times has exponential tail at large arguments, which can be extrapolated as a linear dependence of vorticity in agreement with the isotropic theory by Falkovich - Lebedev (2011).
- A possible reason of isotropization may be related to the nonlocality of the Kraichnan spectrum.

References

1. E.A. Kuznetsov, V.P. Ruban, *Hamiltonian dynamics of vortex lines for systems of the hydrodynamic type*, JETP Letters, **67**, 1076–1081 (1998); *Hamiltonian dynamics of vortex and magnetic lines in the hydrodynamic type models*, Phys. Rev E, **61**, 831–841 (2000); E.A. Kuznetsov,*Vortex line representation for flows of ideal and viscous fluids* , JETP Letters, **76**, 346 –350 (2002).
2. A.N. Kudryavtsev, E.A. Kuznetsov, and E.V. Sereshchenko, *Statistical features of freely decaying two-dimensional hydrodynamic turbulence*, JETP Letters, **96**, 699 – 705 (2013).

References

3. E.A. Kuznetsov, and E.V. Sereshchenko, *Anisotropic characteristics of the Kraichnan direct cascade in two-dimensional hydrodynamic turbulence*, Pisma ZhETF **102**, 870 – 875 (2015) [JETP Letters **102**, 760 – 765 (2016)].

4. E.A. Kuznetsov, and E.V. Sereshchenko, *Isotropization of two-dimensional hydrodynamic turbulence in the direct cascade*, Pisma ZhETF **105**, 70–76 (2017) [JETP Letters **105**, 83–88, (2017)]; arXiv:1702.00738.

THANKS